12-6-1974

An Experimental Investigation of Highly Undercooled Magnesium Silicate Chondrule-Like Spherules

Harry Nicholas Planner

THE UNIVERSITY OF NEW MEXICO
ALBUQUERQUE, NEW MEXICO 87106

Policy on Use of Theses and Dissertations

Unpublished theses and dissertations accepted for master's and doctor's degrees and deposited in the University of New Mexico Library are open to the public for inspection and reference work. *They are to be used only with due regard to the rights of the authors.* The work of other authors should always be given full credit. Avoid quoting in amounts, over and beyond scholarly needs, such as might impair or destroy the property rights and financial benefits of another author.

To afford reasonable safeguards to authors, and consistent with the above principles, anyone quoting from theses and dissertations must observe the following conditions:

1. Direct quotations during the first two years after completion may be made only with the written permission of the author.

2. After a lapse of two years, theses and dissertations may be quoted without specific prior permission in works of original scholarship provided appropriate credit is given in the case of each quotation.

3. Quotations that are complete units in themselves (e.g., complete chapters or sections) in whatever form they may be reproduced and quotations of whatever length presented as primary material for their own sake (as in anthologies or books of readings) ALWAYS require consent of the authors.

4. The quoting author is responsible for determining "fair use" of material he uses.

This thesis/dissertation by Harry Nicholas Planner has been used by the following persons whose signatures attest their acceptance of the above conditions. (A library which borrows this thesis/dissertation for use by its patrons is expected to secure the signature of each user.)

NAME AND ADDRESS	DATE

3/1/73—1M

This thesis, directed and approved by the candidate's committee, has been accepted by the Graduate Committee of The University of New Mexico in partial fulfillment of the requirements for the degree of

Master of Science

An Experimental Investigation of Highly Undercooled Magnesium Silicate Chondrule-like Spherules

Title

Harry Nicholas Planner

Candidate

Geology

Department

David T. Burchfiel

Dean

Dec. 6, 1974

Date

Committee

Dennis Dein

Chairman

Douglas H. Brookins

Albert M. Ludo

AN EXPERIMENTAL INVESTIGATION OF HIGHLY UNDERCOOLED MAGNESIUM SILICATE CHONDRULE-LIKE SPHERULES

by

Harry Nicholas Planner

THESIS

Submitted in Partial Fulfillment of the
Requirements for the Degree of
Master of Science in Geology
in the Graduate School of
The University of New Mexico
Albuquerque, New Mexico

December, 1974

AN EXPERIMENTAL INVESTIGATION OF HIGHLY UNDERCOOLED MAGNESIUM SILICATE CHONDRULE-LIKE SPHERULES

by

Harry Nicholas Planner

ABSTRACT OF THESIS

Submitted in Partial Fulfillment of the
Requirements for the Degree of
Master of Science in Geology
in the Graduate School of
The University of New Mexico
Albuquerque, New Mexico

December, 1974

ACKNOWLEDGMENTS

The author is grateful to Drs. Klaus Keil, Milton Blander (Argonne National Laboratories), and Lloyd S. Nelson (Sandia Laboratories) for allowing him to be actively involved in the experiments and for supplying the magnesium silicate spherules used in this investigation. Thanks is also due Mr. Norman L. Richardson of Sandia Laboratories for his assistance in the laboratory and to Mrs. Sharon Hamilton for typing the manuscript. This work was supported in part by NASA grants NGL 32-004-063 and 32-004-064 (Klaus Keil, principal investigator).

ABSTRACT

A series of experiments, involving molten magnesium silicate spherules that were subjected to high initial cooling rates and allowed to nucleate at high temperatures (985-1350°C), were performed so as to compare their thermal histories to the resulting internal features. Such comparisons could be used to decipher the thermal history of chondrules and the conditions surrounding their formation based on their mineralogy, crystal morphology, and overall texture.

Various features of the spherules were correlated with the initial high cooling rate process, nucleation temperature, and the maximum temperature attained during the recalescance to demonstrate the restrictions resulting from or their sensitivities to specific thermal events. To extend parts of this comparison to spherules nucleating at temperatures lower than those of the high cooling rate experiments (i.e. 800-950°C), several divitrified magnesium silicate spherules were also included in the study.

The only crystalline phase nucleated in these experiments is forsterite despite the fact that the spherules nucleate within the forsterite-protoenstatite field. The residual melt is quenched to a glass. Forsterite crystal morphology changes from a bar-like structure to dendrites, fibers, and submicroscopic crystals, respectively, with greater undercooling for a given bulk composition while the crystal width generally decreases under the same conditions.

The textures of these spherules are of two main classes, spherulitic and those derived from excentroradially arranged, wedge-shaped grains, and can be differentiated on the basis of nucleation temperature and bulk composition. Those spherules consisting of excentroradiating grains appear to be nucleating from the coolest portion of the melt, i. e. near the surface.

Diagrams in which crystal morphology, crystal size, and texture are superimposed on nucleation temperature, with respect to bulk composition, are potential references for determining chondrule nucleation temperatures.

There is a temperature realm in which nucleation of the metastable melt is most likely to occur. Once the nucleation temperature of a chondrule is known, specific parameters can be sought that would restrain nucleation until such undercoolings have been reached, thereby providing a means to test various models that attempt to explain the formation of chondrules.

CONTENTS

FIGURES

Page

TABLES

INTRODUCTION

Chondrules are small spherical bodies, generally less than 2 mm in diameter, largely of silicate composition found embedded in the groundmass matrix of chondritic meteorites and some lunar breccias and fines. They consist of various proportions of the high temperature minerals olivine, pyroxene, and plagioclase which display crystal morphologies that give rise to a variety of internal textures. In addition, minor amounts of metallic nickel-iron, troilite, and other opaques, as well as a glass phase, interstitial to the crystals, may occassionally be detected. Because of their spherical shape, mineralogy, and chemistry, chondrules are generally considered to have formed as isolated systems crystallizing from the molten state.

Chondrules found in lunar samples are considered to have originated from the spray of molten ejecta produced by impact melting of ANT (anorthositic-noritic-troctolitic), KREEP (alkalic high-alumina basaltic) and basaltic rocks on the lunar surface (Frederiksson et al., 1970; Kurat et al., 1971; Keil et al., 1972; King et al., 1972; Kurat et al., 1972).

Meteoritic chondrules, on the other hand, are considered to have formed either as a "primordial" condensate during the evolutionary process of the solar nebula (Wood, 1963a; Blander and Katz, 1967; Blander and Abdel-Gawad, 1969) or through some secondary process involving pre-existing material, such as

volcanism (Tschermak, 1875; Merrill, 1920; Wahl, 1952; Ringwood, 1961; Fredriksson and Ringwood, 1963), impact splattering (Fredriksson, 1963, 1969; Fredriksson and Reid, 1965; Urey, 1967; Kurat et al., 1969), electrical discharges (Whipple, 1966), or shock melting (Wood, 1963b).

Attempts to experimentally synthesize features observed in chondrules were initiated by Rinne (1895, 1897) who was able to produce spherules by melting powders of olivine, hypersthene, and olivine-bronzite mixtures in an electric arc and causing them to splatter explosively.

Experimental investigations into chondrule formation, however, were not continued until more recent times. Synthetic mixtures, similar in composition to the silicate portion of the Bjurböle chondrite, were sealed in platinum tubes with a small amount of water in experiments performed by Frederiksson and Ringwood (1963) and heated until the tubes burst explosively. Salisbury and Fernald (1970) attempted melting dust sized particles in a lightning-like pinched plasma. The experiments of Rinne (1895, 1897) and Fredriksson and Ringwood (1963) produced spherules with internal textures that show a general resemblance to some natural chondrules.

Nelson et al. (1972), unlike previous investigators producing chondrule-like spherules, monitored the temperature of individual molten droplets of either alumina, forsterite, enstatite, forsterite

with albite, or enstatite with albite by means of luminosity-time traces while the droplets were freely falling through various gaseous environments at atmospheric pressure. From their experiments, Nelson et al. (1972) were able to conclude that there are two major factors sensitive to the thermal environment which might affect crystal growth in the resulting metastable molten droplets. These factors are the depth of undercooling before nucleation and the range in temperatures through which the droplet would pass during the recalescence. From these observations they summarized that chondrules are probably the result of spontaneous crystallization of individual molten droplets of metastable undercooled liquids and that the textures produced from those molten droplets which cool in an environment where they are largely undisturbed by heterogeneities, are related mostly to the degree of undercooling, and to a lesser extent to the overall rate of cooling and the temperature of the surrounding environment.

To have the ability, however, to decipher the thermal history of chondrules from their mineralogy, crystal morphology, and overall texture, and to be able to recognize the limitations of such an analysis in the evaluation of various models attempting to explain their formation, more detailed experiments must be performed to examine the effects resulting from the thermal sequence and the physicochemical properties of the material. A series of experiments, involving molten magnesium silicate spherules that

were subjected to high initial cooling rates and allowed to nucleate at high temperatures (985-1350°C), were therefore performed to determine which internal features were most sensitive to specific thermal events or physicochemical properties of the material itself under the conditions provided. The analysis was conducted by correlating various internal features in the spherules with the initial high cooling rate process, nucleation temperatures, and the maximum temperatures attained during the recalescence.

In addition, several glass spherules were devitrified at temperatures of 800-950°C for periods of 20 seconds to 7.23 days to compare their crystal morphology and textures to those spherules nucleating at relatively low temperatures during the high cooling rate experiments mentioned above.

EXPERIMENTAL PROCEEDURE

Since there is a high degree of similarity between meteoritic chondrule bulk composition and the Mg_2SiO_4-SiO_2 system, coupled with the relative simplicity of the system, a starting material of enstatite bulk composition was used in the experiment. The starting material was synthesized from crushed fused silica, shown by spectrographic analysis to contain less than 0.1% impurity, and calcined magnesium carbonate of 99.9% purity. The mixture was melted in an iridium crucible and then repeatedly crushed and remelted.

The experimental arrangement is shown in Fig. 1 and represents a side view with a portion of the furnace cut away. In order to produce a molten droplet from the starting material within a confined space without significantly altering preset ambient conditions, a continuous wave 250 watt CO_2 laser (Model 41, Coherent Radiation Laboratories, Palo Alto, California; smallest spot diameter 1 mm; beam power 5-250 watts; wavelength 10.6 μm) was employed. A modified Marshall model 1510 tubular furnace was utilized to control the high ambient temperature.

The laser and the furnace was aligned such that the laser beam entered the one inch diameter inner tube that extends the length of the furnace and focused on a sample positioned in space at the intersection of this inner tube with two 6 mm diameter viewing ports (labeled as viewing port and access port in Fig. 1) located at the furnace midpoint, 180° apart. The ambient furnace temperature was measured to ±2°C by means of a thermocouple located in a well directly below the one inch diameter inner tube. All experiments were conducted in air at atmospheric pressure.

Small fragments of the starting material were melted onto iridium wire loops of 1 or 1.4 mm diameter by using the focused continuous wave-CO_2 laser beam as a source of heat. The resulting spherules, which are to various degrees elliptical in shape, have average diameters of approximately 1 to 2.5 mm. With the furnace temperature preset to some specific temperature below the liquidus

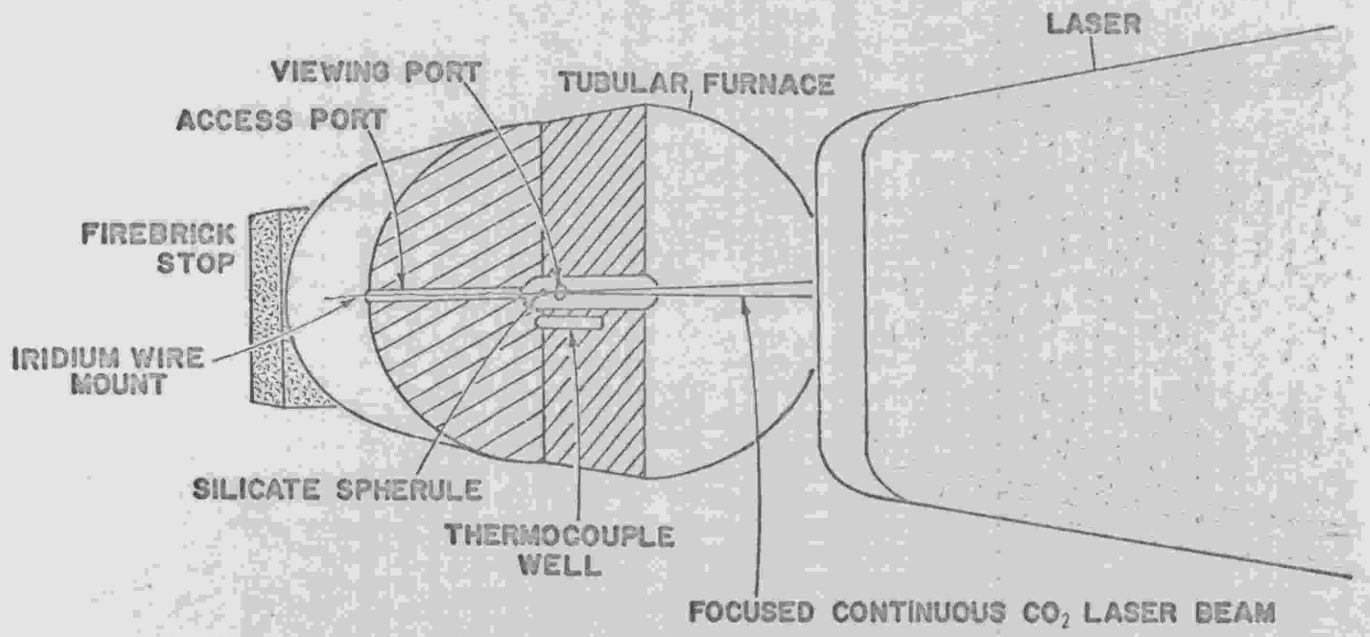

Fig. 1. Schematic diagram of the experimental arrangement. Diagram represents a side view with a portion of the furnace cutaway to show the spatial relationships between sample, laser beam, and the viewing ports.

for an enstatite bulk composition, an individual spherule was positioned in the furnace. Once positioned, laser heating of the spherule commenced. The sample was considered to be completely molten when the visible light radiation of the entire spherule surface was comparable to that at the point of laser impingement, where the material was most undoubtedly molten. Once the sample was entirely molten, laser heating was discontinued and the sample was allowed to cool by radiative and, to a lesser extent, convective heat loss with the temperature of the sample plunging toward the ambient furnace temperature (970-1346°C). As the sample cooled, the visible light radiation decreased in intensity until that point where a recalescence occurred. The duration of time between laser turnoff and the initiation of recalescence and, also the duration of the recalescence were visually estimated and recorded. Immediately following the recalescence, the sample was pulled from the furnace and quenched to room temperature. In addition to the above experiments, four magnesium silicate glass spherules, formed during the preparatory process of the experiment, were placed in furnaces with temperatures in the range of 800-950°C and allowed to devitrify for periods of 20 seconds to 7.23 days (Table 1).

RESULTS

The problem was approached by studying the physicochemical properties associated with fifty-four spherules resulting from the experiments described above. Analytical techniques employed to gather information on these properties include x-ray diffraction analysis, electron microprobe broad and point beam analyses, and optical microscopy. A summary of the data collected with these techniques and of the observations made at the time of the experiment are tabulated in Table 1.

X-Ray Diffraction Analysis

X-ray powder diffraction analysis was used to identify the crystalline phases present in the spherules. X-ray diffraction studies were conducted on finely ground samples with a 114.59 mm diameter x-ray powder diffraction camera using copper radiation with a nickel filter. Exposure periods lasted from three to four hours. Since only that portion of each spherule remaining after thin section preparation could be used for analysis, many samples could not be analyzed for the lack of material.

Analysis of 24 samples (see Table 1) shows that the only detectable phase that had nucleated during the course of the experiment was forsterite.

Table 1. Data collected on the magnesium silicate spherules and observations made at the time of the experiment. Spherules arranged in order of decreasing ambient furnace temperature.

SPHERULE	ELECTRON MICROPROPE BROAD BEAM ANALYSIS (wt %) SiO_2	MgO	Total	X-RAY DIFFRACTION ANALYSIS	AVERAGE DIAMETER (mm)	FURNACE TEMPERATURE (°C)	COOLING TIME BEFORE NUCLEATION (sec)*	DURATION OF RECALESCENCE (sec)*	TEXTURE
EL	49.1	51.0	100.1	fo	1.69	1346	12	>5	P
EK	52.4	48.2	100.6	fo	1.82	1318	17	1-1/2	RG
EM	54.2	45.9	100.1	fo	1.87	1295	15	2	X
EB	50.3	49.8	100.1	fo	(1.99)[1]	1294	>3	n.r.	X
EI	50.5	49.8	100.3	fo	1.82	1290	6-7	2	P
EH	49.6	50.5	100.1	n.a.	1.55	1271	4-1/2	(rapid)	X
EP	52.4	48.2	100.6	n.a.	2.55	1266	13	1	R
EN	52.2	47.3	99.5	fo	2.34	1259	8	1	RG
EQ	55.1	44.2	99.3	fo	2.25	1248	13	1	RG
EC	47.0	53.0	100.0	n.a.	(1.78)[1]	1240	4	(slow)	X
ER	54.6	45.2	99.8	fo	2.24	1234	11	2	P
E13	49.8	50.5	99.8	n.a.	1.31	1220	5	2-2-1/2	X
ET	53.4	46.0	99.4	n.a.	2.20	1191	9	4-5	P
E7	53.0	46.6	99.6	n.a.	1.54	1186	5	2	X
ED	54.4	45.8	100.2	fo	1.74	1186	10	>1	R
E5	55.8	45.1	100.9	n.a.	1.82	1179	4	2	P
EG	50.4	49.4	99.8	fo	2.13	1173	10	(slow)	X
E4	53.0	47.7	100.7	n.a.	1.53	1173	4-1/2	1	RG
E20	53.8	46.1	99.9[2]	n.a.	1.34	1162	5	2-1/2	X
E21	53.5	45.4	98.9[2]	n.a.	1.23	1162	7-1/2	3	S
E3	52.0	48.0	100.0	fo	1.82	1147	5	(slow)	RG
E18	54.4	45.2	99.6	n.a.	1.50	1145	4-1/2	2	X, P
E1	48.9	50.4	99.3	n.a.	1.93	1143	5	(rapid)	P
E2	51.1	48.8	99.9	fo	1.52	1141	5	(rapid)	X
23E1	43.9	56.2	100.1	n.a.	1.16	1140	2	n.r.	P(?)
E26	54.4	45.8	100.2	fo	1.37	1128	8-1/2	3	S
23E2	52.6	46.8	99.4	fo	1.55	1119	4	1	X
EE	47.9	51.4	99.3	n.a.	(1.64)[1]	1118	3	1/2	X
23E3	46.4	54.7	101.1	fo	1.47	1113	2	1/2	X, P
23E4	48.7	51.8	100.5	fo	1.74	1110	7-1/2	1	P
23E5	46.5	53.6	100.1[2,3]	fo	1.49	1106	4	2	P
23E6	48.6	50.0	98.6[2]	n.a.	1.47	1068	3-1/2	2	P
23E7	51.5	48.0	99.5	n.a.	1.49	1066	3	3	P
23E8	46.4	54.1	100.5	n.a.	1.14	1056	4	1	R(?)
23E9	49.8	50.5	100.3	fo	1.78	1054	3	3	P
23E12	48.4	51.5	99.5	n.a.	1.18	1042	3-1/2	2	R
24E1	48.7	51.3	100.0	fo	0.94	1003	3	1-1/2-2	X
24E4	48.9	51.0	99.9[3]	n.a.	1.25	1003	4	1	X
24E2	51.3	48.3	99.6[3]	fo	1.03	1003	4-1/4	1	R
24E3	52.0	48.1	100.1	n.a.	1.12	1003	5	1	X
24E5	53.0	48.0	101.0	fo	1.64	1003	5	1	X
24E6	48.7	51.4	100.1	fo	1.23	1002	4	1	R
24E7	48.7	51.0	99.7	fo	1.35	1002	4-1/2	2	R
24E8	52.9	47.0	99.9	n.a.	1.07	997	5	1-1/2	S
24E10	52.5	47.8	100.3	n.a.	1.18	989	4-1/2	1	X
24E9	55.2	45.3	100.5[3]	n.a.	1.03	989	16	2	S
24E11	53.9	45.6	99.5[3]	n.a.	1.21	986	5-1/4	1-1/2	R
24E12	54.1	45.9	100.0	fo	1.41	982	10-1/4	2	S
24E13	53.1	46.9	100.0	n.a.	1.44	973	9	1-1/4+	S
24E14	49.3	49.9	99.2	n.a.	0.98	970	4-1/2	1	X
DEVITRIFIED SPHERULES									†
MB6	58.6	39.5	98.1[2]	n.a.	(1.11)[1]	950	---	---	S 20 sec.
MB5	57.8	41.3	99.1	n.a.	(1.04)[1]	924	---	---	S 2.25 min.
MB1	56.8	43.3	100.1	n.a.	(1.16)[1]	800	---	---	S 43.5 hrs.
MB2	59.7	40.7	100.4	n.a.	(1.14)[1]	800	---	---	S 7.23 days

EXPLANATION

( )[1] average diameter measured from thin section

)[2] thin section surface contains numerous cracks and voids

)[3] center of spherule richer in MgO than along periphery

* visual estimation

† divitrification period

n.a. not analyzed

n.r. not recorded

fo forsterite

X exceutroradial texture

R radial texture

S spherulitic texture

P parallel grain texture

RG random grain texture

Optical Microscopy

It would be unfeasible to describe in detail each of the fifty four spherules used in this study. Examination of each of the spherules shows, however, that most of the features observed in thin-section can be categorized.

Textures

The texture is considered to be the overall shape and arrangement of the grains within any of these spherules. The size and morphology of the crystals, constituting any of the grains, has no appreciable affect on how the spherule is classified according to texture. Figs. 2 through 6 provide what is believed to be a representative sampling of textures displayed in the magnesium silicate spherules. These textures are classed as either radial, excentroradial, spherulitic, parallel grains, or as random grains. Radial (Fig. 2) and excentroradial (Fig. 3) textures describe crystals diverging from the center and peripheral regions of the spherule, respectively. Those spherules which contain numerous spherulitic bodies, each of which is composed of radiating crystal "fibers", are termed spherulitic (Fig. 4). The parallel grain texture is here described as long, approximately trapezoidal grains oriented parallel to each other or to sets of parallel oriented trapezoidal grains that are at some angle to each other. Textures described as random grains consist of short, stubby grains that have little or no orientational relationship to other grains within the spherule.

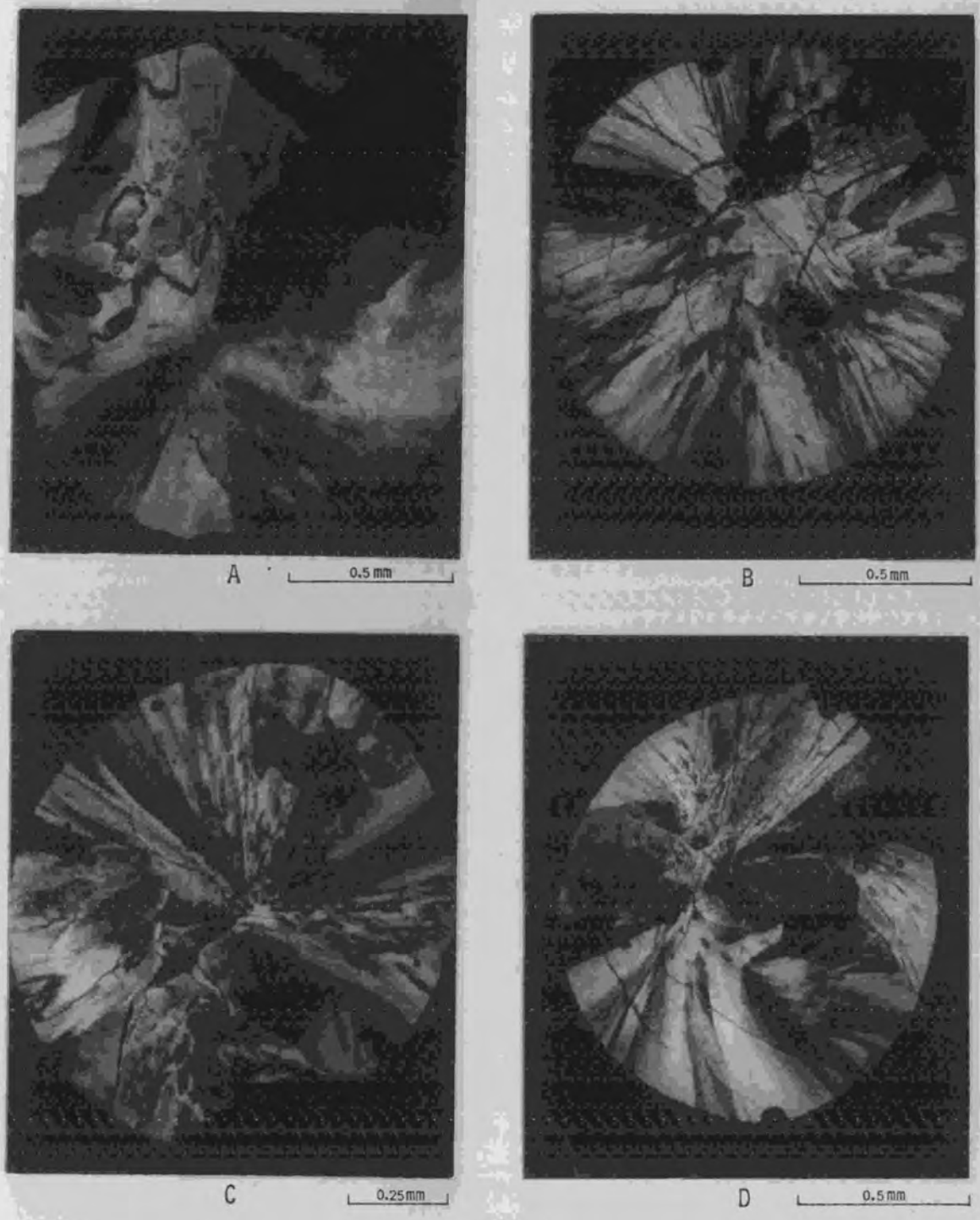

Fig. 2. Photomicrographs of selected magnesium silicate spherules displaying a radial texture. Spherules shown are: (2a) EP; (2b) 24E7; (2c) 24E6; and (2d) 23E12. Curved grains are displayed in spherule 23E12 (2d). Crossed nicols.

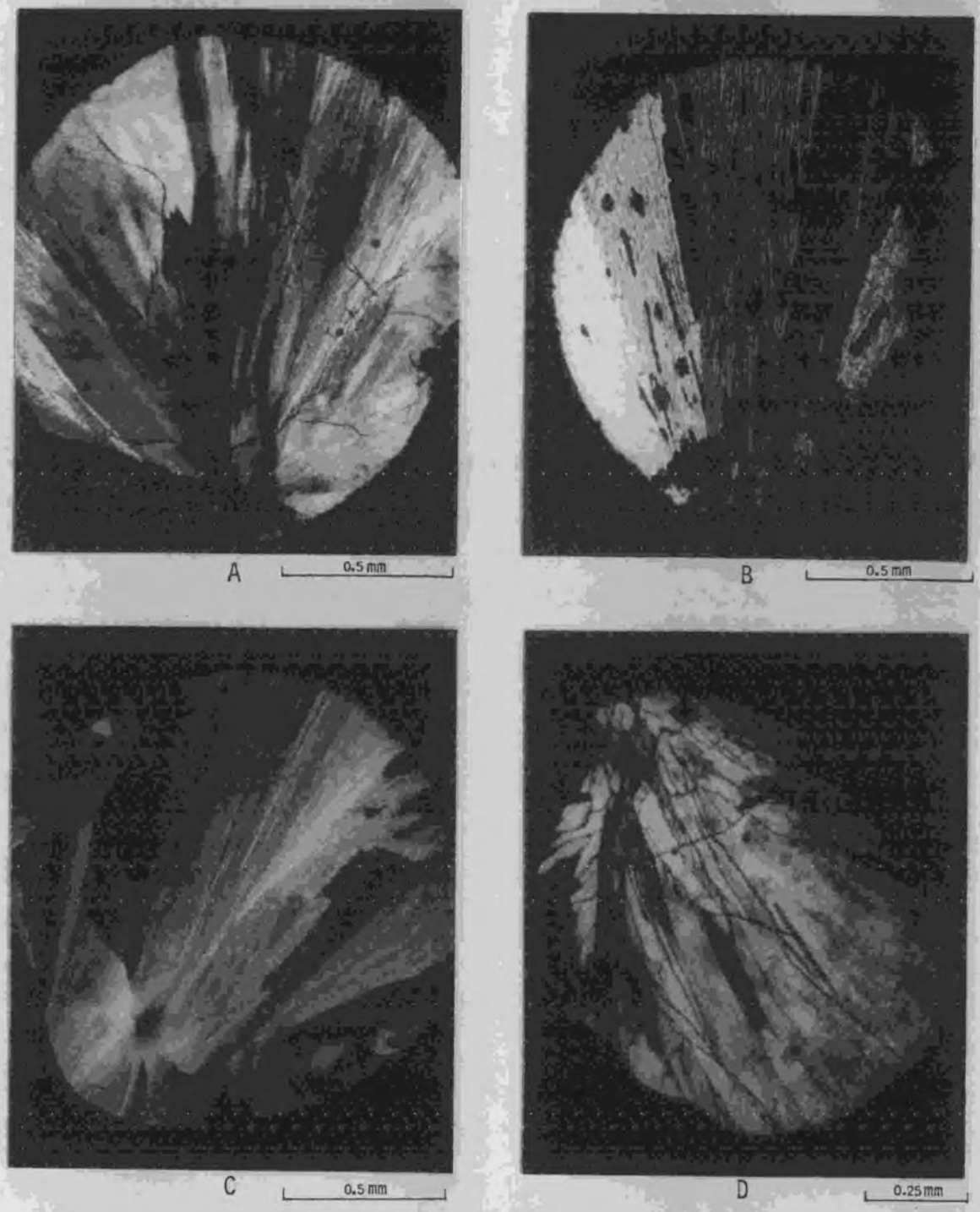

Fig. 3. Photomicrographs of selected magnesium silicate spherules displaying an excentroradial texture. Spherules shown are: (3a) 23E2; (3b) EG; (3c) EM; and (3d) 24E3. Crossed nicols.

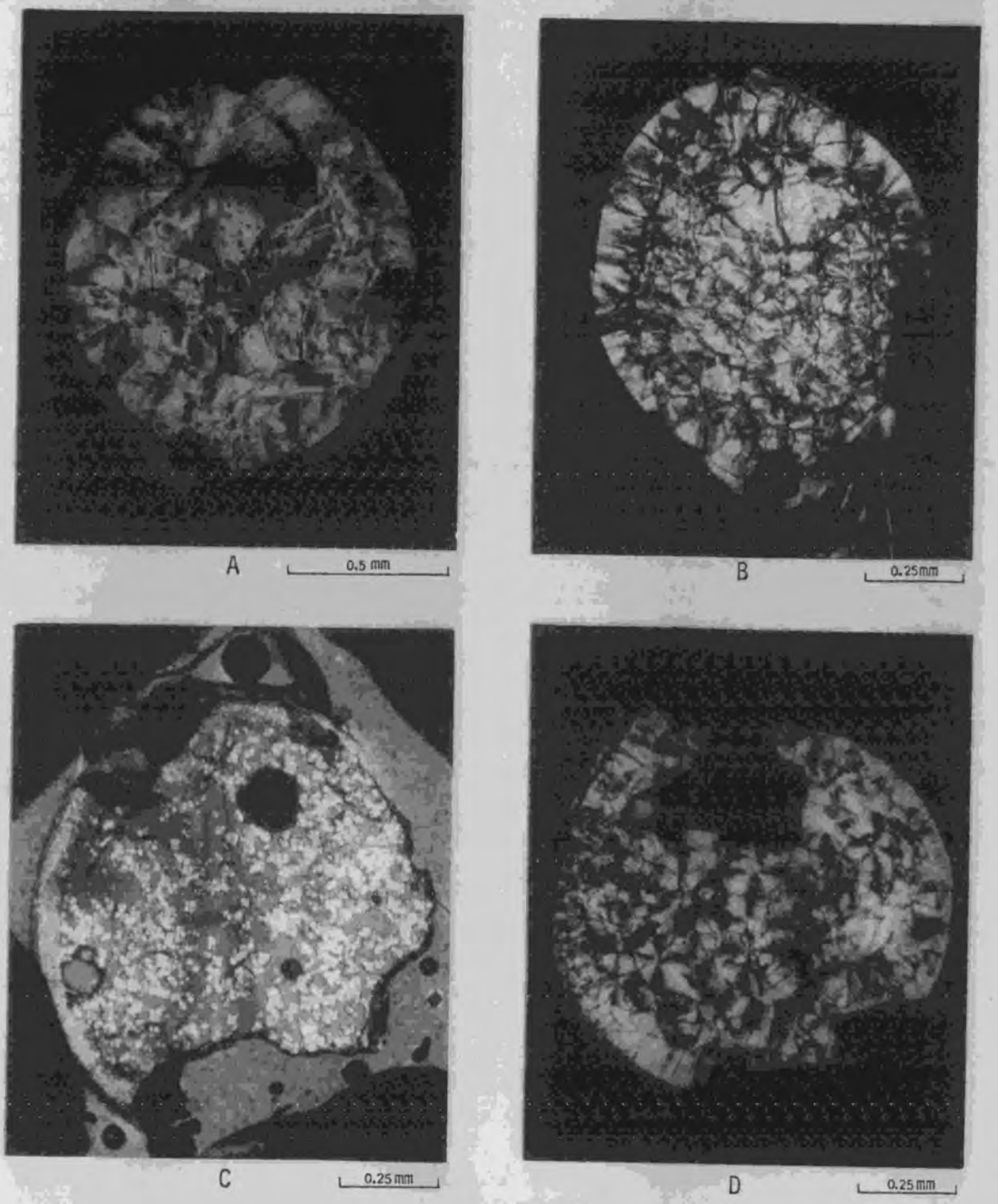

Fig. 4. Photomicrographs of selected magnesium silicate spherules displaying a spherulitic texture. Spherules 24E12 (4a) and 24E9 (4b) were produced from the high cooling rate experiments. MB2 (4c) and MB6 (4d) are devitrified glass spherules. Nicols crossed in 4a, b, and d. Nicols partially crossed in 4c.

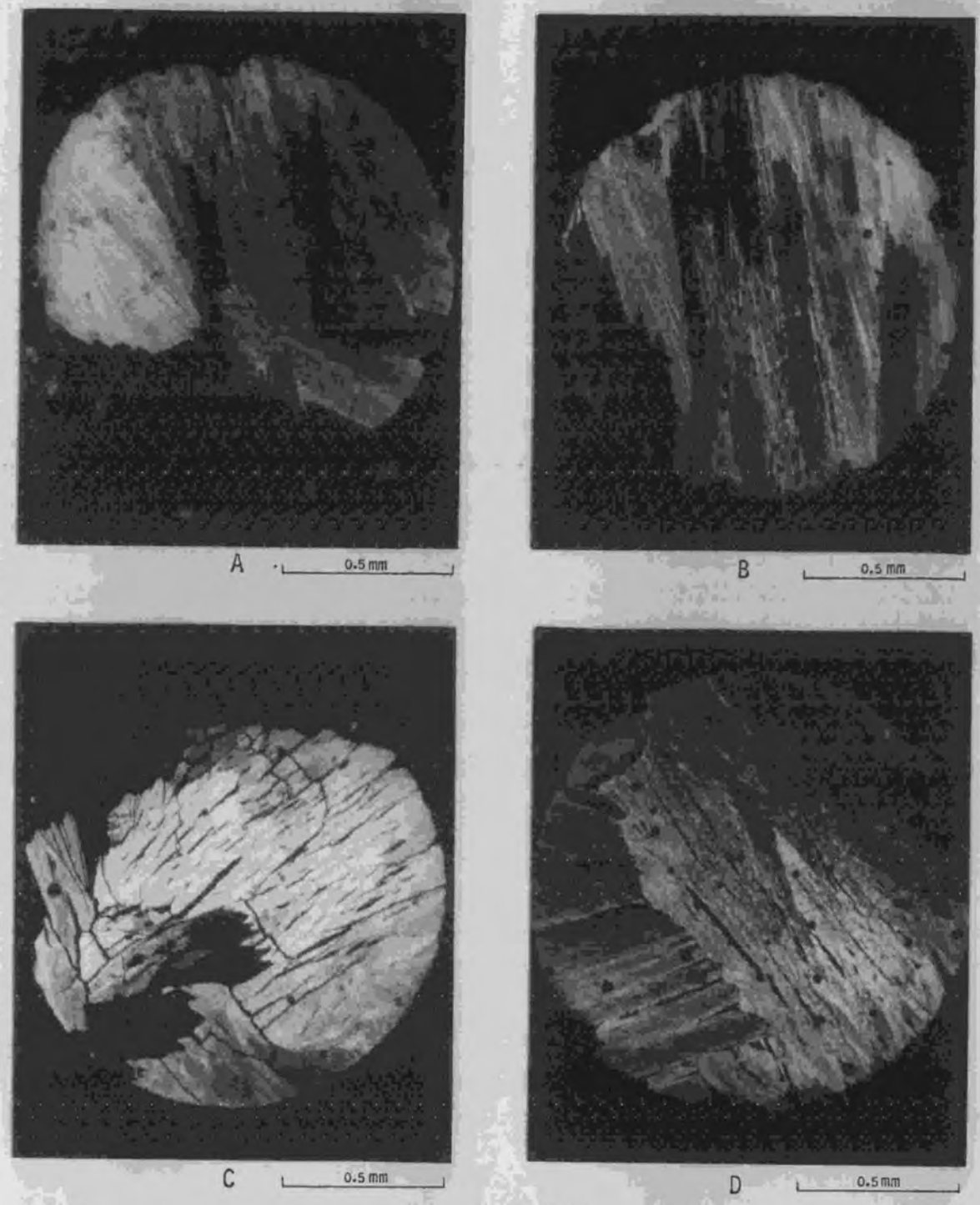

Fig. 5. Photomicrographs of selected magnesium silicate spherules displaying a parallel grain texture. Spherules shown are: (5a) 23E7; (5b) E5; (5c) 23E4; and (5d) 23E9. Crossed nicols.

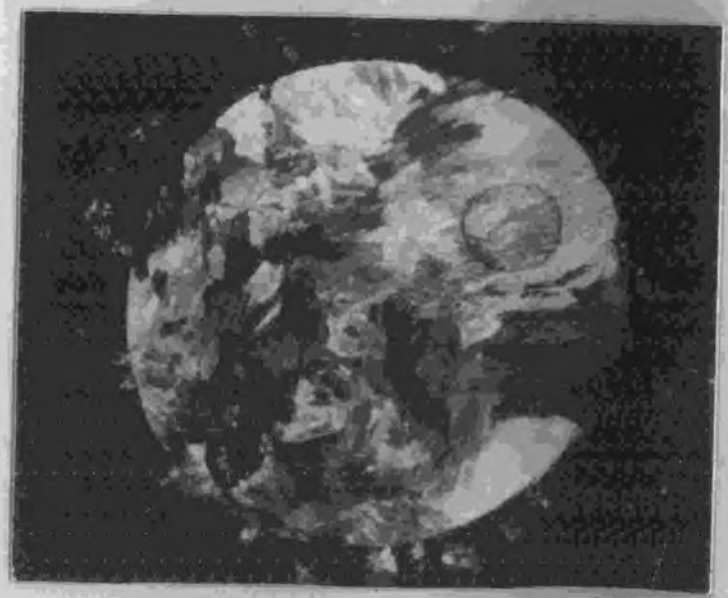

A

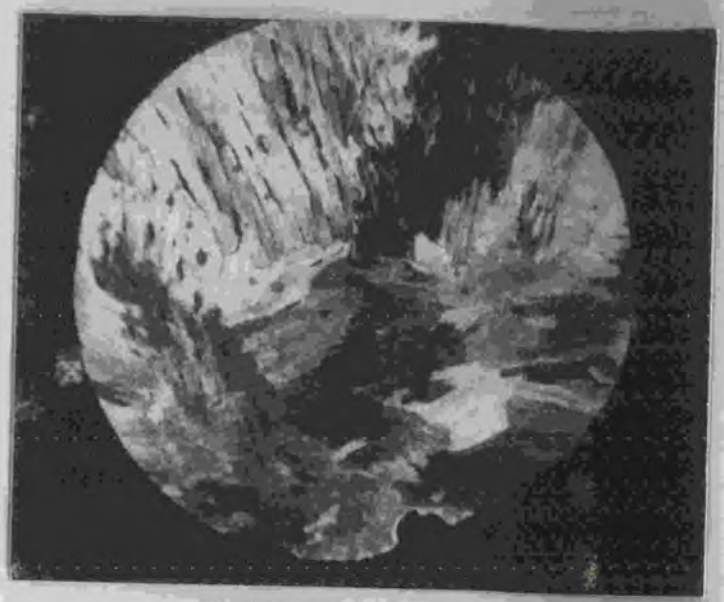

B

Fig. 6. Photomicrographs of selected magnesium silicate spherules displaying a random grain texture. Spherules shown are: (6a) E4; and (6b) EK. Crossed nicols.

The textural classification for each spherule is provided in Table 1. The most prominent textures resulting from the experimental conditions previously described are excentroradial and those displaying parallel grains. To a lesser extent are the spherulitic, radial, and random grain textures, in that order. The fact that parallel grain textures can be generated from a spherule displaying an excentroradial texture will be demonstrated in the discussion.

Grains within the Spherules

Grains in these spherules are considered as an aggregate of forsterite crystals of similar continuous array. Their shapes are most commonly wedge, trapezoidal, or platelet forms. For grains displaying a wedge or trapezoidal shape, the longest dimension of the crystals within the grain correspond, in general, to the longest dimension of the grain. There are some wedge shaped grains that exhibit a curved feature (e.g. Fig. 2d) corresponding to the curved nature of the crystals within.

Where grain boundaries are distinct, they are usually irregular or interlocking, but in many cases, actual grain boundaries are difficult to define. This appears not only to be a function of the true nature of the boundary (irregular or interlocking) but also as a result of only slight changes in crystal orientation in adjacent grains.

All grains display an undulatory extinction. For platelets, this may be more accurately described as mosaic extinction.

Nucleation Center for the Excentroradial Texture

For spherules displaying an excentroradial texture, it appears that nucleation occurs at or near the surface or along the iridium wire-melt interface. It should be noted, however, that minute unattached spheres of iridium observed within spherules EB and ET did not act as nucleation centers.

Devitrified Spherules

For the devitrified spherules, each spherulite can be considered as a grain. Figure 7 shows details of the spherulitic texture and of the rims in spherules MB2 and MB6. Spherulites in MB1, 2, and 5 are suspended in a glass matrix whereas those in MB6 have developed to the point where each spherulite is in contact with surrounding spherulites. Rim structures in the devitrified spherules, when present, are composed of sub-microscopic crystals radiating from the surface, a feature not observed in spherules resulting directly from the high cooling rate experiments that also display a spherulitic texture.

Crystal Morphology

Forsterite crystal morphology, as displayed in the magnesium silicate spherules, can be classed as either bars, dendrites, fibers, or as submicroscopic crystals. Cross-sectional views through these crystals suggest that the faces bounding the sides of the crystal have a subrounded outline.

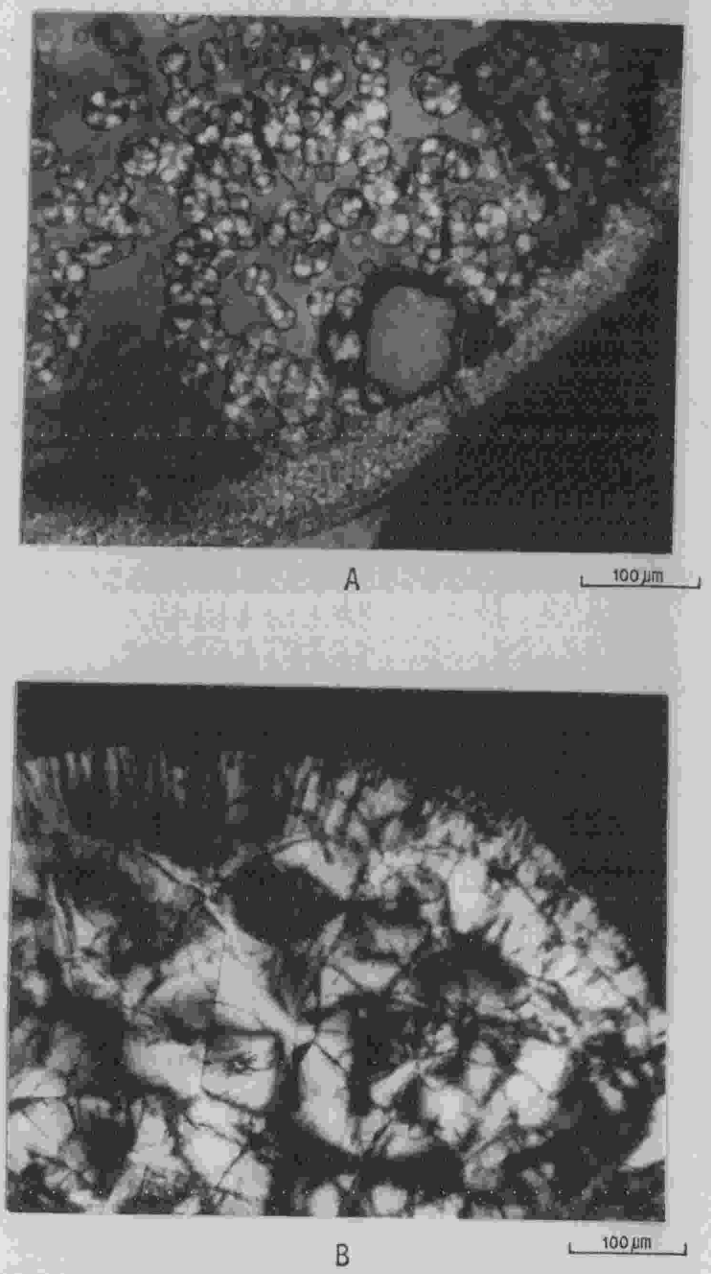

Fig. 7. Photomicrographs of devitrified glass spherules showing details of the spherulitic texture and of the rims. Nicols crossed in 7b (spherule MB6) and partially crossed in 7a (spherule MB2).

Forsterite crystal bars are almost exclusively of a skeletal nature, that is, hollow or incomplete. Examples of skeletal bars are given in Figs. 8a-c. The skeletal feature extends the length of the bar and may appear as a series of irregularly spaced circular holes (CH, Figs. 8a and 8b), ovoid structures (OS, Figs. 8a and 8b), or as a line structure that may or may not contain circular holes (LS, Figs. 8a-c). The development of the first two structures can be implied from the change in the crystal habit along the length of the bar. The origin of these habits is obviously derived from crystal dendrite growth. The development of the line structure, however, is not apparent. The only clue to its formation might be that of a dendrite structure displayed in Fig. 8d. Each of the three skeletal habits can appear in the same spherule and, often, along the same train of skeletal bars.

Forsterite crystal dendrites also display a variety of habits, as can be seen from Figs. 9a and 9b. The basic structure of the dendrite is similar to that of a comb. The "back" of the comb represents the "body" of the crystal and the teeth, extending from the back of the comb at right angles to it and all in the same plane represents the actual dendrite extensions. The dendritic extensions may be short and stubby (Figs. 9a and 10a) or thin and long (Fig. 9b). The dendrite habit of Fig. 9a may not be readily apparent, although this thin-section pattern can be formed in numerous ways. Two such methods can be visually explained by

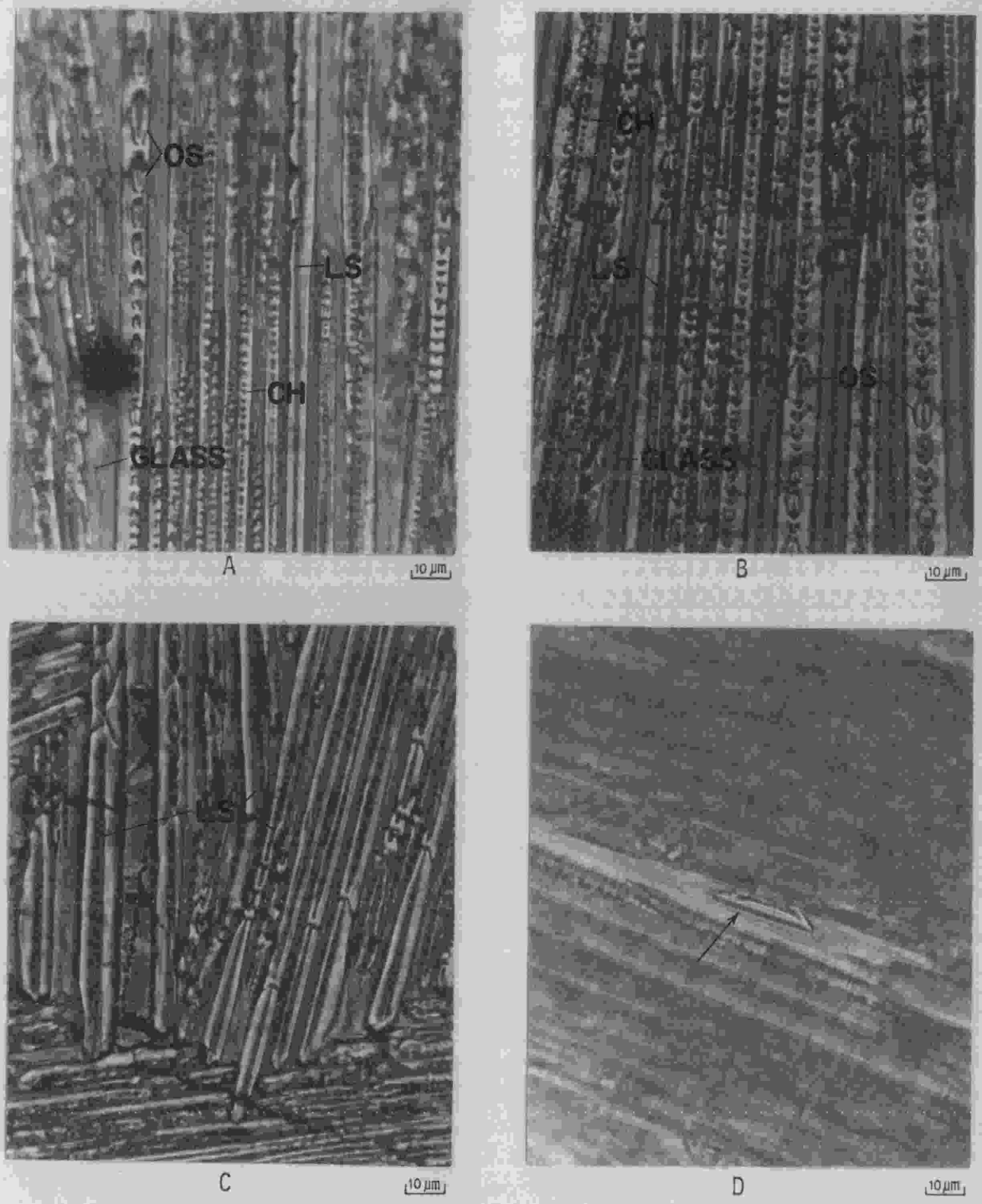

Fig. 8. Skeletal structures displayed in forsterire bars. CH, circular holes; OS, ovoid structures; and LS, line structures. Dendrite habit in 8d may represent link between dendrites and those forsterite bars displaying a line structure. Transmitted polarized light.

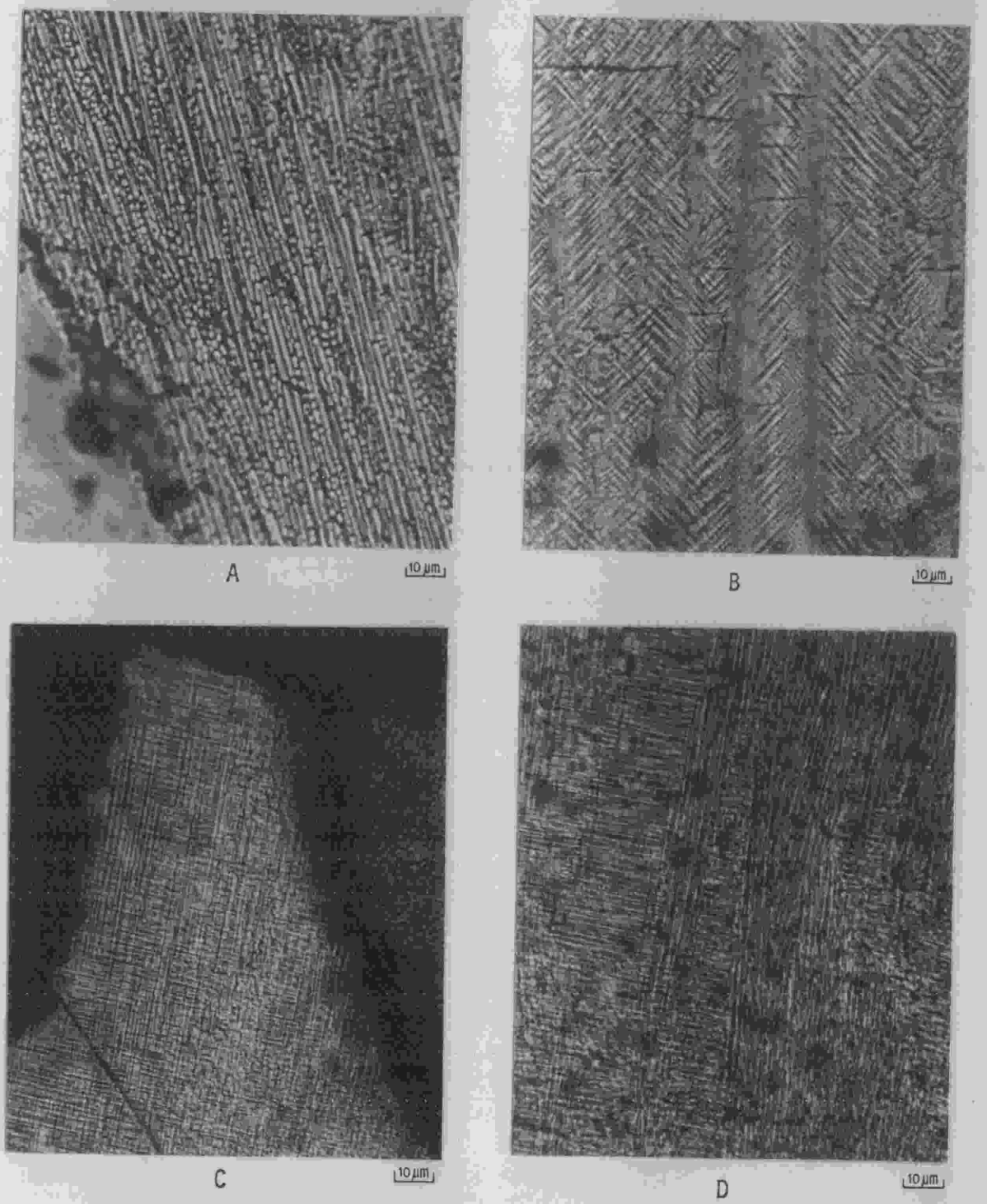

Fig. 9. Forsterite dendrite forms (9a and b) and the two varieties of dendrite mesh (9c and d). Photomicrographs 9a and b in transmitted polarized light; 9c and d with crossed nicols.

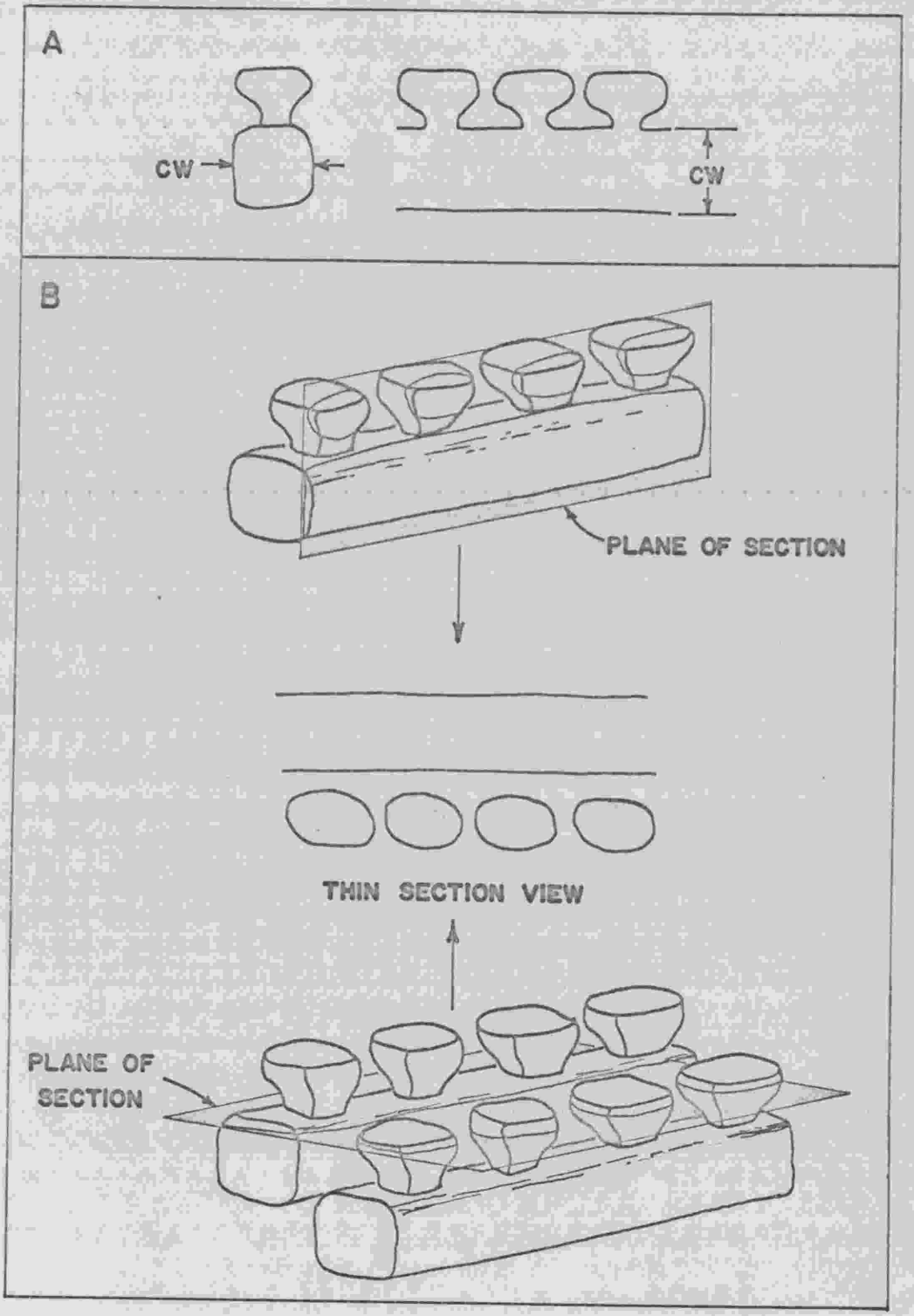

Fig. 10. Diagrams of the short stubby forsterite dendrite form. Cross sectional views shown in 10a. CW corresponds to that dimension used to determine the crystal width (or crystal size) of a dendrite. Two possible means of producing the thin section view in Fig. 9a are presented in 10b.

Fig. 10b. Other methods for deriving this pattern result from dendrites being inclined to some degree with respect to the plane of the section.

Those dendrites with long, thin extensions will often align their "bodies" parallel to each other and form sheet-like structures with the dendrites extending in the same plane as the sheet. Two types of mesh result and are displayed in Figs. 9c and d. The geometric relation between the two mesh habits, if there is one, is unknown.

Forsterite fibers appear as single thread-like structures that often display some degree of curvature. The fibers may parallel each other or in some instances form a mesh-like habit similar to Fig. 9d. It has not been concluded for crystal fibers that actual dendrites are responsible for the latter habit.

In several of the excentroradial spherules displaying the nucleation center, crystal morphology can be seen to make a gradation from submicroscopic crystals to skeletal bars along a traverse leading away from the nucleation center. Fig. 11 demonstrates such a trend viewed in spherule 24E14. This provides evidence that crystal morphologies grade into adjacent morphological classes.

The crystal morphologies for each of the spherules is summarized in Table 2.

Fig. 11. Gradation in crystal morphology from forsterite fibers to dendrites with increasing distance from the nucleation center. Transmitted polarized light.

Table 2. Summary of forsterite crystal morphologies and sizes observed in the magnesium silicate spherules.

SPHERULE	CRYSTAL MORPHOLOGY	CRYSTAL SIZE	SPHERULE	CRYSTAL MORPHOLOGY	CRYSTAL SIZE
EB	1, 2	4	23E2	1, 2, 3	10
EC	1, 2	6	23E3	2	6
ED	1, 2, 3	6	23E4	1, 2	5
EE	1, 2	6	23E5	2	
EG	1	26	23E6	1, 2	4
EH	1, 2		23E7	1, 2	5
EI	1, 2	4	23E8	2	
EK	1, 2	5	23E9	1, 2	10
EL	1, 2	4	23E12	2, 3	
EM	1, 2	10	24E1	2	
EN	1, 2	6	24E2	2, 3	
EP	1, 2	4	24E3	2, 3	
EQ	1, 2	6	24E4	2, 3	
ER	1, 2	3	24E5	2, 3	
ET	1, 2	10	24E6	2	
E1	1, 2	3	24E7	2	
E2	1, 2		24E8	1, 2, 3	
E3	1, 2	4	24E9	3, 4	
E4	1, 2	4	24E10	2, 3	
E5	1, 2	8	24E11	2, 3	
E7	1, 2, 3, 4	7	24E12	3, 4	
E13	2		24E13	3, 4	
E18	1, 2, 3	4	24E14	2, 3	
E20	1, 2, 3	3	MB1	4	
E21	2, 3, 4		MB2	4	
E26	2, 3		MB5	4	
23E1	1, 2	14	MB6	4	

EXPLANATION

CRYSTAL MORPHOLOGY

1 bars

2 dendrites

3 fibers

4 (submicroscopic crystals)

CRYSTAL SIZE

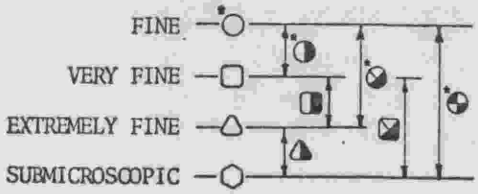

* number represents greatest crystal width observed

arrows indicate range in crystal size

Crystal Size

Any crystal size determinations, as to establish a classification for the spherules based on the size of the crystals within, must consider the following.

The length of the crystal can not be used as a measurement of size because of the difficulty in determining where any one crystal terminates. Secondly, any crystal lying in a plane other than that of the thin-section will appear shorter than it really is. Since the cross-sectional outline of the crystal may be subrounded, a measurement of the crystal width has the advantage of being little affected by its orientation with respect to the plane of the thin section, however, a standardized approach must be considered in the measuring of all crystal dendrites. The crystal width of a dendrite will be taken as the width of the dendrite "body" as shown in Fig. 10a.

Based on an observation that specific crystal widths correspond to the limits of certain crystal morphologies, crystal size is classified according to crystal width into four groups:

crystal size class	crystal width
fine	>2 μm
very fine	0.5-2 μm
extremely fine	(submicroscopic)-0.5 μm
submicroscopic	submicroscopic

The correlation between crystal size (width) and crystal morphology, as it has been defined in this study, is shown in Fig. 12. The division in crystal width at 0.5 μm corresponds to the transition of crystal fibers to obvious dendrites. The division established at a 2 μm crystal width corresponds to the appearance of skeletal bars.

Each of the crystal width classifications is continuous with its adjacent group(s) forming a continuum of crystal widths from sub-microscopic to approximately 26 μm for the magnesium silicate spherules of the present study. The greatest crystal width, approximately 26 μm, is not believed to represent a physical maximum in the bar morphology.

The crystal width classes for each of the spherules is summarized in Table 2, where it becomes immediately obvious that a large percentage of the spherules contain more than one crystal size classification.

Glass Phase

Microscopy of spherules with 'fine' and 'very fine' crystal sizes often reveal the presence of a glass phase. In spherules displaying crystal bars, the glass is most readily observed as a brown-tinted material surrounding each skeletal forsterite bar as a rind (Figs. 8a-c). It also seems to be detectable as an optically darker phase in polarized reflected light as interstitial material to 'fine' crystal dendrites and interstitial to the sheets of 'very fine' mesh-habit crystals.

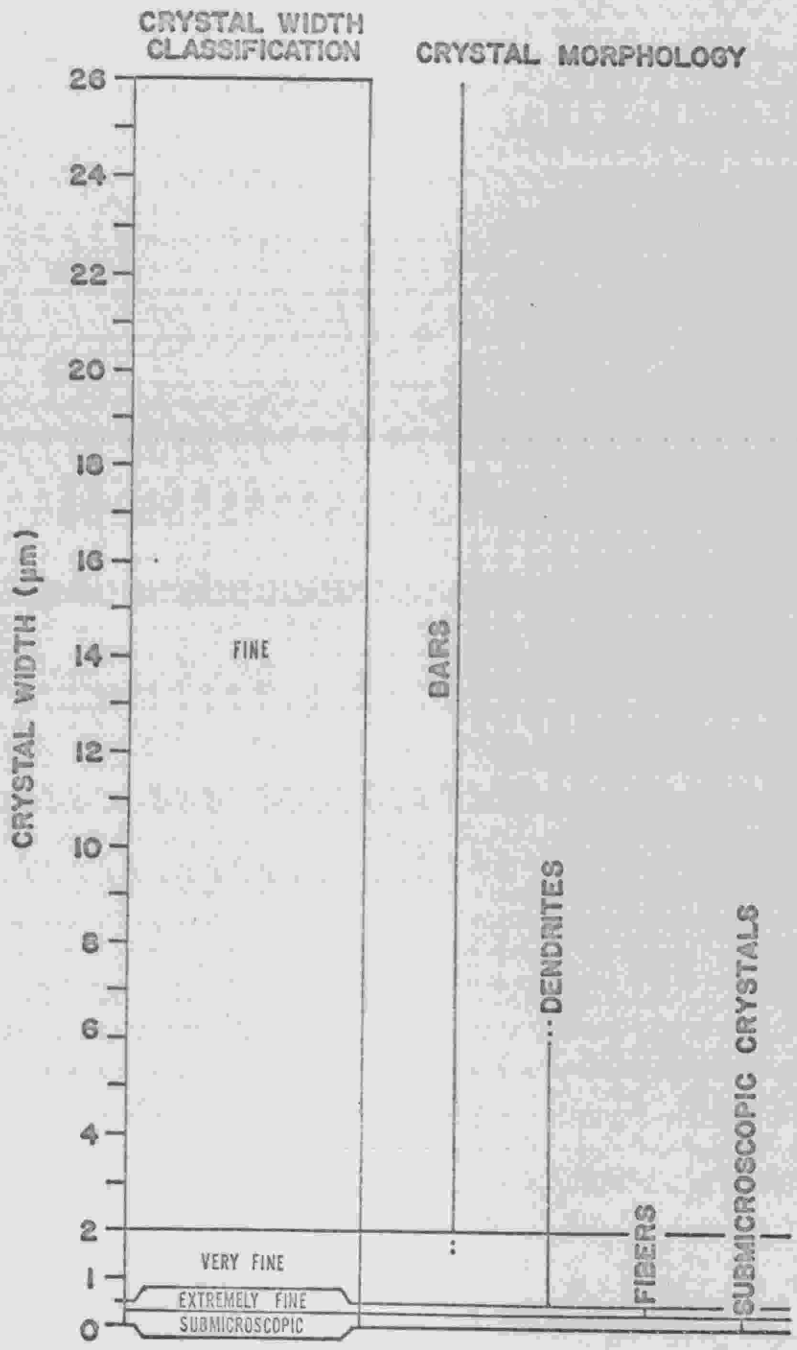

Fig. 12. Correlation between crystal width, crystal width classification, and the crystal morphology for forsterite crystals in the magnesium silicate spherules.

Under crossed nicols, the glass phase appears isotropic only in a few cases where it occupies a relatively larger sectional area than is normally observed. Otherwise, it appears anisotropic, going extinct at the same moment as neighboring forsterite crystals or may approach total extinction, as just described, but display a feather-like appearance. The former is most probably the result of the presence of forsterite in the same optic path as the glass and the feathery feature is due to the presence of submicroscopic crystals of forsterite within the glass.

Voids within the Spherules

Voids are common in the spherules and are generally long, thin and have smooth outlines. They are located between forsterite skeletal bars or at grain boundaries. They are most abundant and reach their greatest size near the central region of the spherule, when present, and often extend in one direction toward the spherule's surface. They are believed to result from the expelling of gases, that were dissolved in the melt, as the spherule crystallized. Spherules displaying a spherulitic texture usually contain numerous cracks and voids within the spherulites. This latter feature is thought to result from the change in specific volume as forsterite crystallizes from a glass phase.

Electron Microprobe Analysis

The broad beam electron microprobe techniques of Prinz et al. (1971) was employed to determine the bulk composition of each spherule. In the current study, the beam was broadened within a range of 30 to 150 μm, depending on sample size and the arrangement and density of cracks and voids.

The composition of the glass phase, which was determined in several spherules, was obtained by point beam electron microprobe analysis.

Enstatite of known composition served as a standard. Both types of analyses were corrected for instrumental effects (drift, deadtime, and background) according to Keil (1967) and differential matrix effects as outlined by Bence and Albee (1968) and Albee and Ray (1970).

Bulk analyses made on polished thin sections of each of the fifty-four spherules and, also, the starting material showed that the majority of the spherules are considerably homogeneous in composition. For those spherules that display an inhomogeneity in composition, it usually appeared as a silica enrichment around the periphery of the spherule.

Electron microprobe bulk analysis shows that laser heating of the spherules to produce a molten droplet creates serious vaporization loss of silicon over magnesium. The resulting spherules, which had

initially contained 59.9 wt % SiO_2, have silica compositions in the range of 43.9 to 55.6 wt % (Table 1). The devitrified glass spherules show a much smaller silica variation, 56.8 to 59.7 wt %. It should be noted that the latter underwent but one laser heating episode of relatively short duration. The distribution of spherule compositions are displayed in Fig. 13 as a function of magnesia content.

Because of severe overlap problems with forsterite, point beam analysis of the glass phase could only be obtained from seven of the fifty spherules resulting directly from the high cooling rate experiment. For those seven spherules, the glass phase was discovered to be of identical composition, corresponding to the eutetic composition of the Mg_2SiO_4-SiO_2 binary (65 wt % SiO_2, 35 wt % MgO; Bowen and Andersen, 1914), despite differences in bulk spherule composition. The analyses are presented in Table 3.

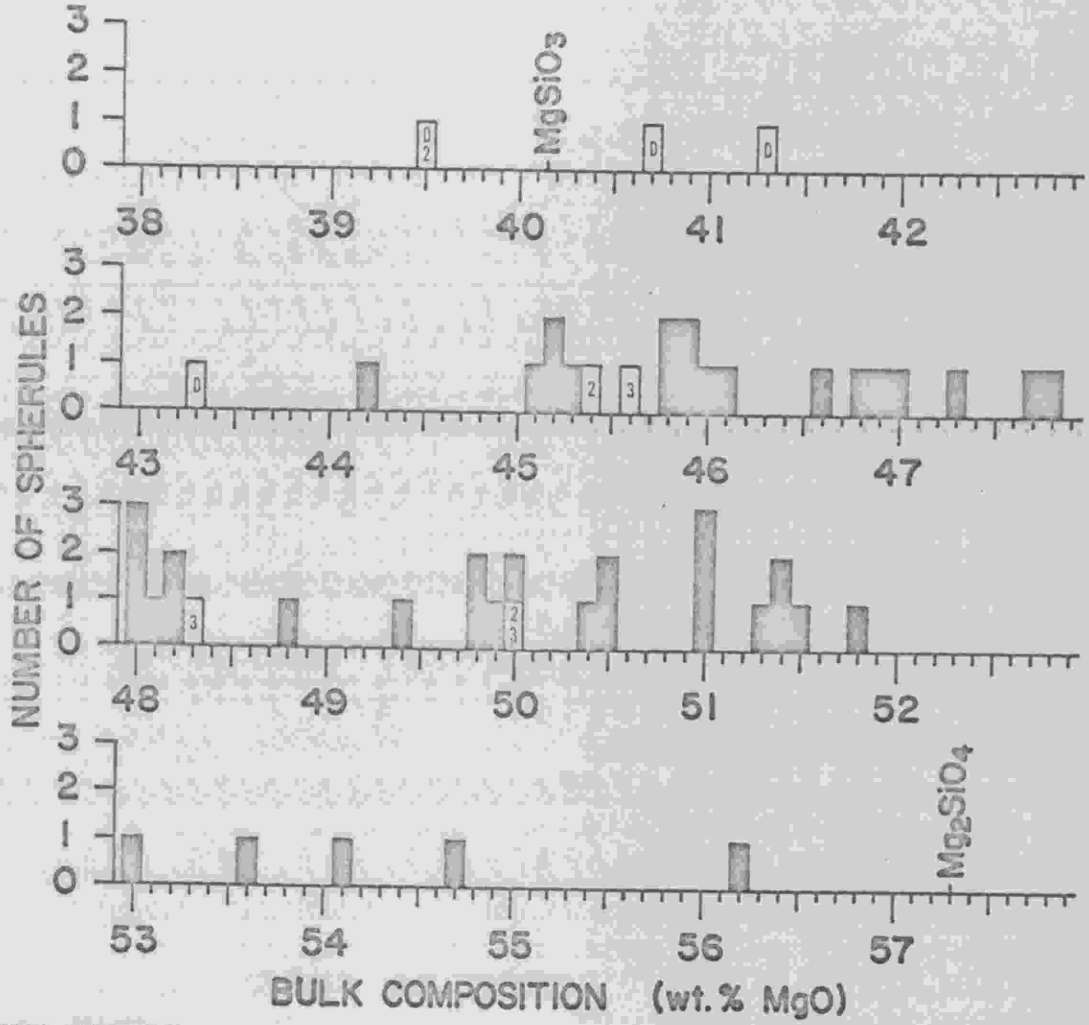

Fig. 13. Distribution of spherule bulk composition as a function of magnesia content.

Table 3. Electron microprobe analysis of the glass phase in seven magnesium silicate spherules.

SPHERULE	SPHERULE BULK COMPOSITION (wt %)			GLASS COMPOSITION (wt %) AVERAGE			RANGE	
	SiO_2	MgO	Total	SiO_2	MgO	Total	SiO_2	MgO
E5	55.8	45.1	100.9	65.6	34.7	100.3	65.2-66.0	33.4-35.2
24E11	53.9	45.6	99.5	65.2	35.0	100.2	65.0-65.4	34.4-35.5
EM	54.2	45.9	100.1	65.3	34.3	99.6	64.7-66.8	33.4-35.1
ET	53.4	46.0	99.4	65.4	34.4	99.8	64.7-66.2	33.5-35.2
23E2	52.6	46.8	99.4	65.6	34.6	100.2	65.6-65.7	34.3-34.9
23E7	51.5	48.0	99.5	65.2	34.7	100.3		
EG	50.4	49.4	99.8	65.2	34.6	99.8	64.5-65.7	33.8-35.4

DISCUSSION

The cooling history of a spherical droplet during the experiment can best be exemplified with Fig. 14. This figure is a photograph taken of an oscilliscope screen displaying the luminosity of a magnesium silicate droplet, as detected by a photomultiplier tube filtered for 6590Å radiation, as a function of time. Since the luminosity of this trace and the temperature of the spherule can be related by means of Planks' relation, the trace provides an excellent means of visualizing the temperature variation of the spherule during the experiment.

At laser turnoff, as a result of radiative and, to a lesser extent, convective heat transfer from the spherule's surface to the surroundings, the temperature of the droplet plunges rapidly toward the ambient temperature. The spherule will continue to approach the ambient temperature until a crystalline phase is nucleated. Nucleation initiates a brief recalescence resulting from the release of the heat of fusion as crystals grow from the melt. Thereafter, the temperature of the spherule immediately decreases again, approaching the ambient temperature.

It is the above thermal history that must be evaluated in conjunction with the features observed within each of the spherules so that the thermal history of chondrules may be understood and constraints on their possible modes of formation set forth. The major parameters that must be evaluated so that a thorough examination

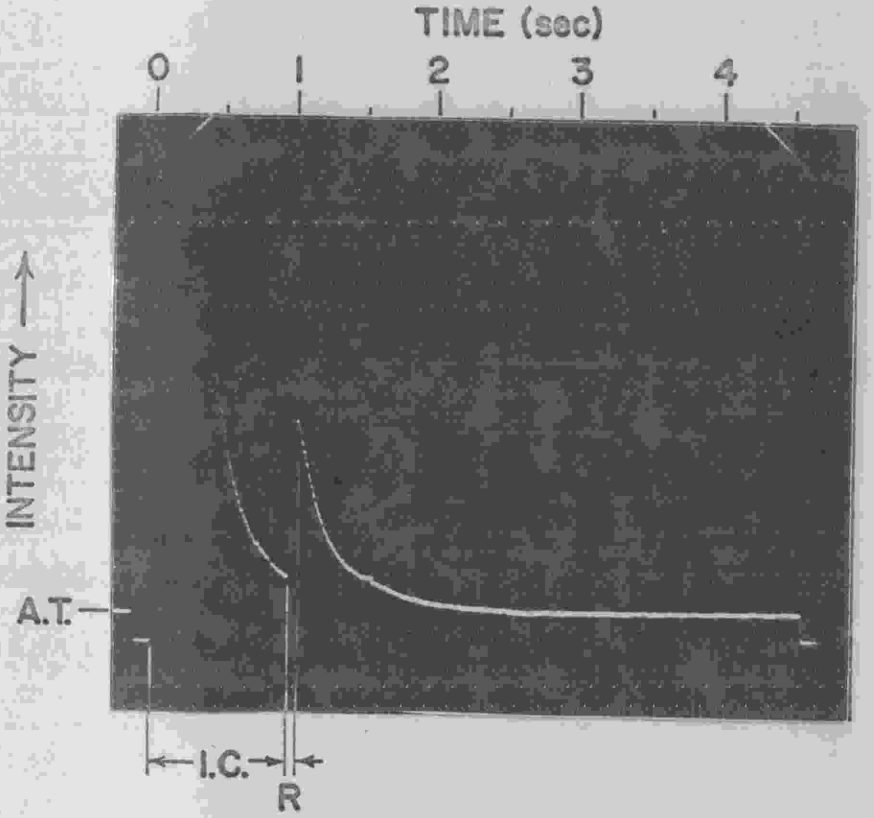

EXPLANATION

A.T. - AMBIENT TEMPERATURE

I.C. - INITIAL COOLING PROCESS (Duration: 0.98 sec)

R - RECALESCENCE (Duration: 65 msec)

Fig. 14. Luminosity-time trace exemplifying the cooling history of a magnesium silicate spherule during the experiment.

might proceede are: 1) the thermal history of the spherule up to the time of nucleation of a crystalline phase; and 2) the thermal history of the recalescence. The former allows an estimation of the cooling rate, degree of undercooling, and conditions surrounding nucleation. The later allows for a comparison between its thermal history and crystal size, crystal morphology, and the mineralogy within a spherule.

Luminosity-time traces represent an accurate means to record the temperature of a spherule at any given time, assuming that the temperature of the spherule is nearly uniform throughout. This is especially true since the experiment requires high temperatures and sample isolation, and, also, involves extremely short lived thermal features. Since the thermal events of each of the spherules consists merely of visual estimations, recorded at the time of the experiment, various other methods must be introduced to define the temperatures at any point or interval of interest.

The remainder of the discussion is broken into several sections surrounding specific aspects of the thermal history.

Initial Cooling Process

Temperature Estimation

The initial cooling history may be approached from the stand point of an energy balance. At any time, τ, the rate of decrease of energy content in a spherule is equal to the rate of energy loss from its

surface. Assuming that energy loss at the surface of a spherule will occur by radiation heat loss only and, secondly, that the temperature within the spherule will be approximately uniform at any given time, the time lapsed after laser turnoff as a function of the temperature of the spherule is calculated as follows:

The relationship between the amount of heat transferred from a substance and its corresponding change in temperature is given by

$$dQ = m\ Cp\ dT \tag{1}$$

where Q is the heat transfer across the boundary of the system, i.e. the surface of the spherule; m is the mass; Cp is the specific heat at constant pressure, and T is the absolute temperature. Replacing m with the product of the volume of the spherule, V, and its density ρ, gives

$$dQ = \rho\ V\ Cp\ dT \tag{2}$$

The rate of heat transfer that corresponds to the cooling rate of the spherule, is, therefore

$$\frac{dQ}{d\tau} = \rho\ V\ Cp\ \frac{dT}{d\tau} \tag{3}$$

The rate of heat transfer by radiation at the surface of the spherule (Sears and Zemansky, 1967) is given by

$$\frac{dQ}{d\tau} = A\varepsilon\sigma\,(T^4 - T_o^4)$$

where A is the surface area; ε is the relative emittance of the surface; σ is a universal constant (13.55×10^{-13} cal / sec cm^2 K^4); and T_o is the ambient furnace temperature.

Equating the rate of energy loss by radiation at the surface to the change in temperature of the spherule gives

$$-\rho\ V\ Cp\left(\frac{dT}{d\tau}\right) = A\varepsilon\sigma\ (T^4 - T_o^4). \qquad (5)$$

The negative sign is included because $dT/d\tau$ is negative in this case.

Equation 5 can be rewritten to give

$$d\tau = -\frac{V\rho Cp}{A\varepsilon\sigma} \cdot \frac{dT}{(-T_o^4 + T^4)} .$$

Assuming that ρ, Cp, V and A are independent of temperature, integration from the initial conditions to some τ and T after laser turnoff produces the relationship

$$\int_0^{\tau} d\tau = -\frac{V\rho Cp}{A\varepsilon\sigma} \int_{T_i}^{T} \frac{dT}{((-T_o)^4 + T^4)} \qquad (7)$$

$$\tau = -\frac{V\rho Cp}{A\varepsilon\sigma}\left[-\frac{1}{2T_o^3}\left[\frac{1}{2}\left(\ln\frac{T+T_o}{T-T_o} - \ln\frac{T_i+T_o}{T_i-T_o}\right) + \tan^{-1}\frac{T}{T_o} - \tan^{-1}\frac{T_i}{T_o}\right]\right] \qquad (8)$$

$$\tau = \frac{r\rho Cp}{6\varepsilon\sigma T_o^3}\left[\frac{1}{2}\ln\left(\frac{T+T_o}{T-T_o} \Big/ \frac{T_i+T_o}{T_i-T_o}\right) + \tan^{-1}\frac{T}{T_o} - \tan^{-1}\frac{T_i}{T_o}\right] \qquad (9)$$

where r is the radius of a sphere. Equation 9 gives the time after laser turnoff as a function of the temperature for $T_i \geq T > T_o$.

To be able to apply this equation to the spherules resulting from the experiment, values for r, ρ, Cp, ε and T_i must now be considered.

As discussed previously, the spherules are not true spheres, but are elliptical to various degrees. Despite the eccentricity, at least two orthogonal axes of the spherules (one coinciding with the longest axis) have been measured to obtain an average diameter which in turn is used to estimate the radius.

Density and coefficient of volume expansion measurements obtained by Tomlinson et al. (1958) for magnesium silicate melts have been used to obtain densities for melts in the 1300-1900°C range. These densities are plotted in Fig. 15 and extended to cover the range in composition of interest. The densities for forsterite and orthoenstatite, 3.22 and 3.209 g/cm^3, respectively, are significantly greater than their corresponding melts, although for a range in temperature of 900°C, the density of the melt varies only ~ 0.16 g/cm^3. The value that will be considered the density for a particular spherule will correspond to that temperature that is median to its initial and ambient temperatures for the appropriate composition according to Fig. 15.

Melts with a forsterite or enstatite composition both have specific heat values of 0.348 cal/g K, according to Barin and Knacke (1973). Since the magnesium silicate melts are intermediate to these compositions their specific heats also correspond to this value.

The relative emittances for the compositions being dealt with were not measured at the time the experiment was performed. As a result, only a rough approximation can be assumed. According to Sparrow and Cess (1970), for electric nonconductors appearing white to the eye, the emittance of the sample is generally quite high in the infrared range. Therefore, after comparison with other materials that are classified similarly, it is not totally

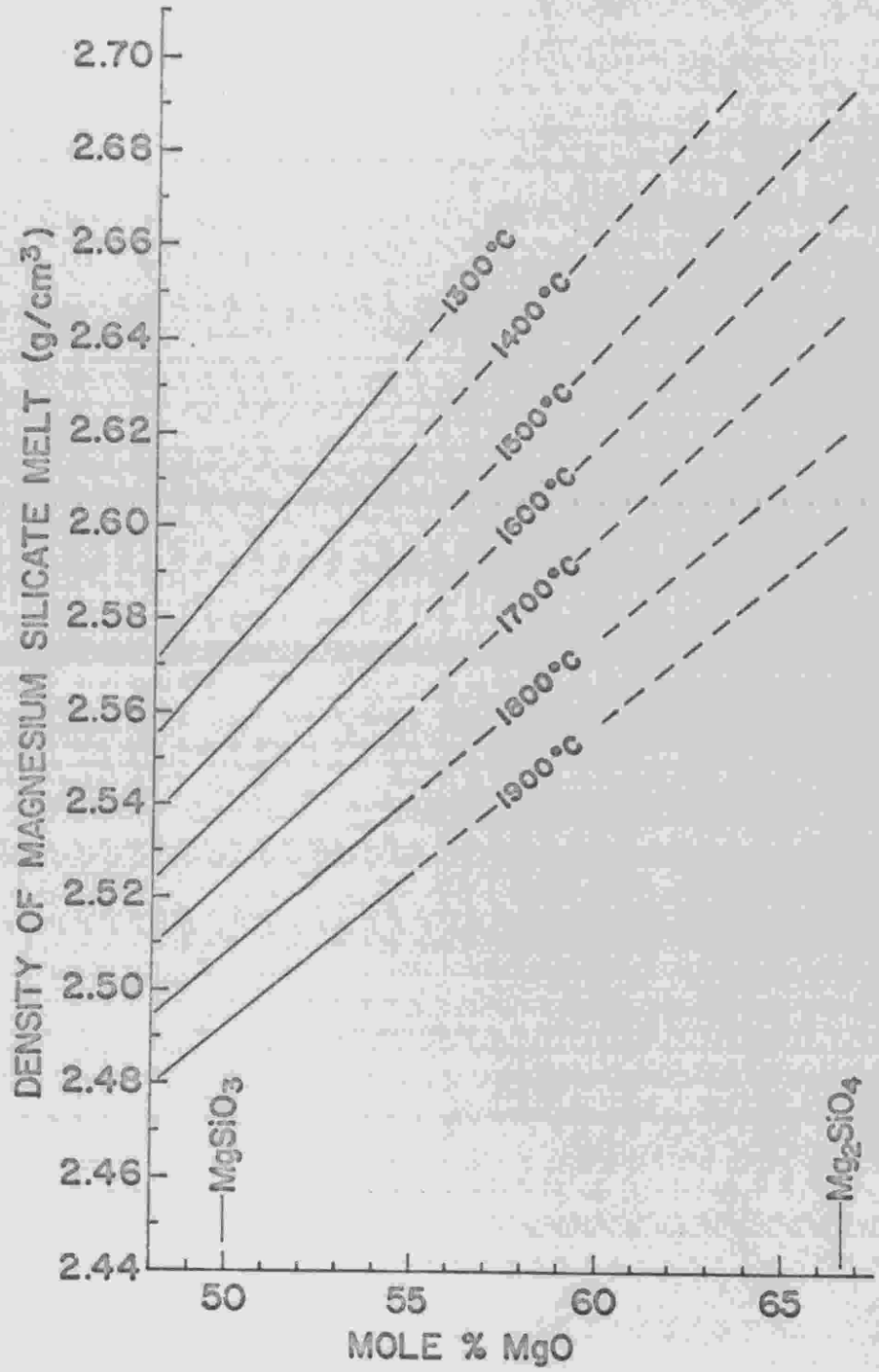

Fig. 15. Densities for magnesium silicate melts with compositions in the range 48 to 67 mole % MgO and for temperatures between 1300 and 1900°C (after Tomlinson et al., 1958). Dashed lines represent an extrapolation to more forsteritic compositions.

unreasonable to assign a value of 0.8 to the relative emittance, although this does lead to the largest uncertainty among the parameters considered here to be constants.

Similarly, the initial temperature of the spherules are not known directly from the experiments. Figs. 16a and b represent cooling curves for 1 and 2 mm diameter spherules, respectively, calculated from Equation 9 using two different initial temperatures (1600 and 2000°C) and two different ambient temperatures representing the extremes of the experiment. It can be seen from Fig. 16a that at any time greater than ~ 2 seconds, the temperature difference between the two cooling curves for a 1 mm diameter spherule and a specific ambient condition is less than 30°C despite a 400°C difference in the initial temperature assumed. This temperature difference, however, does increase for larger spherules (see Fig. 16b). It is believed that the initial temperature of the spherule may be taken as the equilibrium liquidus temperature, for a given spherule, plus 100°C without introducing considerable error to the temperature determination.

Before applying Equation 9 to the experimental data, Figs. 16a and b offer additional information as to the accuracy of the temperature estimates. If some thermal event occurred after laser turnoff and was recorded visually at, say, 2 seconds and for another, 7 seconds and allowing a half or even a one second error (±), it

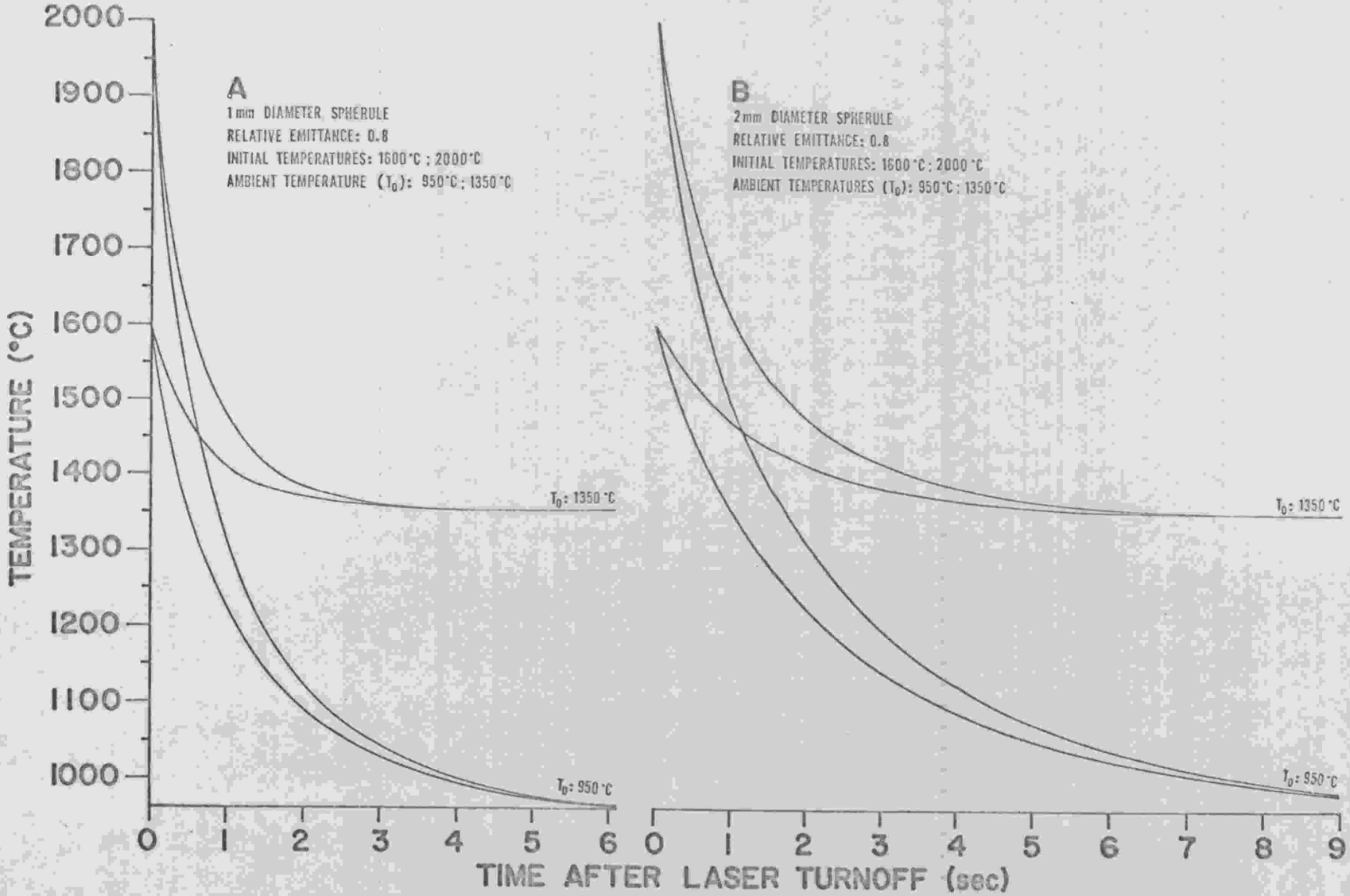

Fig. 16. Cooling rate curves for 1 mm (16a) and 2 mm (16b) diameter spherules calculated from Eq. 9.

can be seen from these figures that the error in corresponding temperature estimates is much more severe at the shorter estimated time interval.

Despite all of the best estimates that have been provided here, the temperature estimates that follow should be viewed with some caution. General conclusions can be sought, but more definitive arguments can not be established based on the experimental data that are provided.

Nucleation Temperatures

Nucleation temperatures, calculated from Equation 9 using the estimated cooling times shown in Table 1, are given in Table 4. These temperatures range from 985-1346°C and their distribution with respect to spherule bulk composition is provided by Fig. 17. From this diagram it is evident that nucleation can occur at lower temperatures for a more enstatite-rich composition. If the degree of undercooling (the temperature difference between that of the metastable melt and the equilibrium liquidus) is considered, however, all spherules are confined to undercoolings in the range 400-800°C despite the variation in composition (see Fig. 17).

The importance of the nucleation temperature and, consequently, the degree of undercooling is the fact that growth rate is also a function of these parameters. The nucleation temperature, therefore, places the nucleated crystalline phase with respect to its growth rate at the time of nucleation. These are the initial conditions for subsequent crystal growth.

Table 4. Nucleation temperatures and undercoolings acquired by the magnesium silicate spherules resulting from the high cooling rate experiments. Spherules arranged in order of decreasing ambient furnace temperature.

SPHERULE	COMPOSITION (wt % MgO)	AMBIENT FURNACE TEMPERATURE (°C)	EQUILIBRIUM LIQUIDUS TEMPERATURE (°C)	ESTIMATED COOLING TIME (sec)	ESTIMATED NUCLEATION TEMPERATURE (°C)	UNDERCOOLING (°C)
EL	51.0	1346	1797	12	1346	451
EK	48.2	1318	1746	17	1318	428
EM	45.9	1295	1704	15	1295	409
EB	49.8	1294	1776	>3	--	--
EI	49.8	1290	1776	6-7	1300	476
EH	50.5	1271	1788	4-1/2	1289	499
EP	48.2	1266	1746	13	1268	478
EN	47.3	1259	1730	8	1269	461
EQ	44.2	1248	1670	13	1249	421
EC	53.0	1240	1830	4	1285	545
ER	45.2	1234	1689	11	1237	452
E13	50.0	1220	1780	5	1231	549
ET	46.0	1191	1706	9	1200	506
E7	46.6	1186	1734	7	1207	527
ED	45.8	1186	1702	10	1188	514
E5	45.1	1179	1688	4	1233	455
EG	49.4	1173	1770	10	1180	590
E4	47.7	1173	1737	4-1/2	1204	533
E20	46.1	1162	1707	5	1177	530
E21	45.4	1162	1694	7-1/2	1164	530
E3	48.0	1147	1743	5	1189	554
E18	45.2	1145	1689	4-1/2	1177	512
E1	50.4	1143	1787	5	1194	593
E2	48.8	1141	1758	5	1167	591
23E1	56.2	1140	1875	2	1257	618
E26	45.8	1128	1702	8-1/2	1131	571
23E2	46.8	1119	1722	4	1174	548
EE	51.4	1118	1805	3	1229	576
23E3	54.7	1113	1855	2	1291	564
23E4	51.8	1110	1811	7-1/2	1126	685
23E5	53.6	1106	1839	4	1165	674
23E6	50.0	1068	1780	3-1/2	1154	626
23E7	48.0	1066	1743	3	1175	568
23E8	54.1	1056	1846	4	1099	747
23E9	50.5	1054	1789	3	1207	582
23E12	51.1	1042	1799	3-1/2	1106	693
24E1	51.3	1003	1803	3	1070	733
24E4	51.0	1003	1797	4	1070	727
24E2	48.3	1003	1749	4-1/4	1039	710
24E3	48.1	1003	1745	5	1033	712
24E5	48.0	1003	1743	5	1072	671
24E6	51.4	1002	1755	4	1066	689
24E7	51.0	1002	1797	4-1/2	1062	735
24E8	47.0	997	1730	5	1022	708
24E10	47.8	989	1740	4-1/2	1036	704
24E9	45.3	989	1692	16	989	703
24E11	45.6	986	1696	5-1/4	1019	677
24E12	45.9	982	1704	10-1/4	989	715
24E13	46.9	973	1723	9	985	738
24E14	49.9	970	1778	4-1/2	1004	774

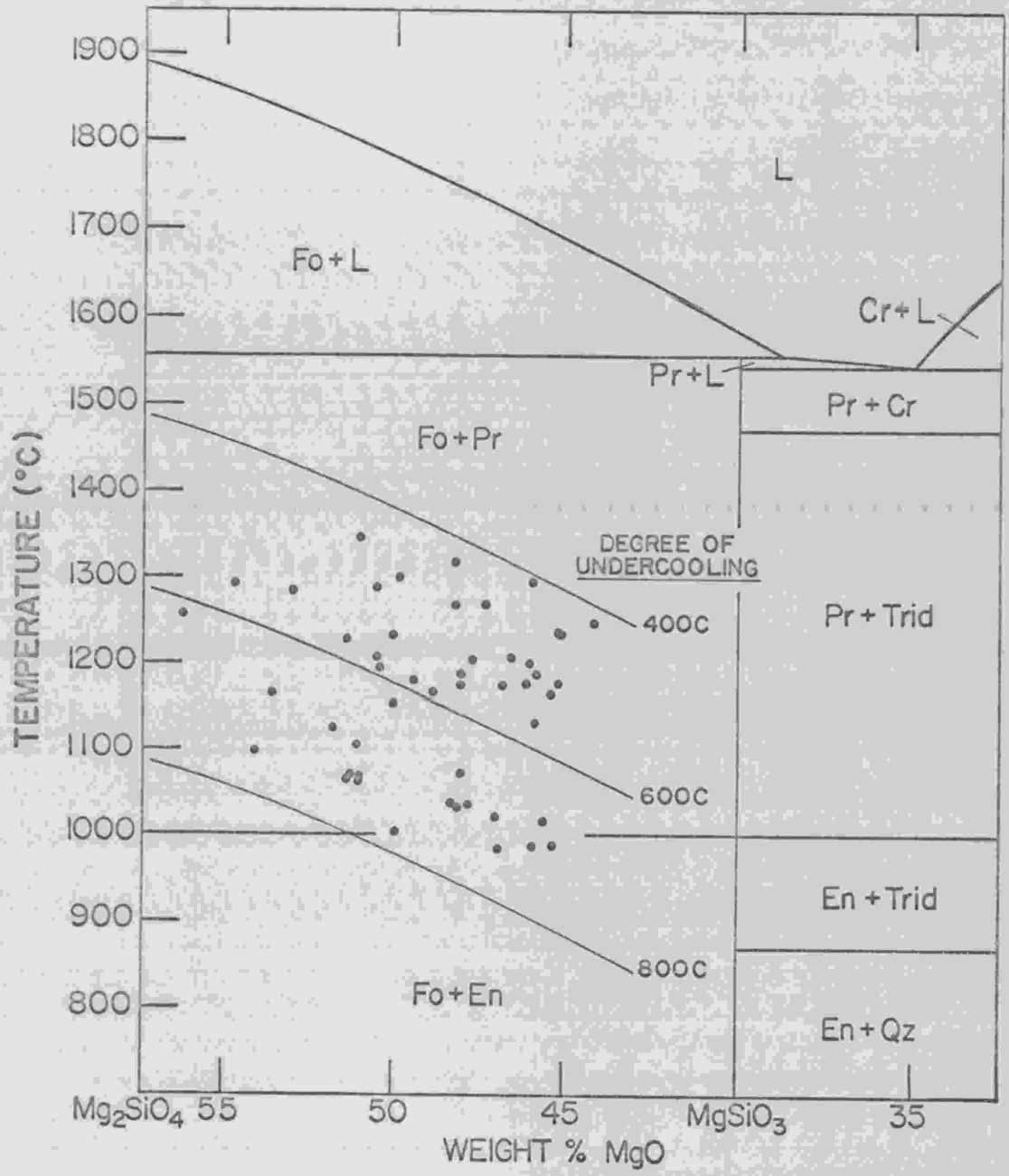

Fig. 17. Estimated nucleation temperatures of magnesium silicate spherules resulting from the high cooling rate experiments. Equilibrium phase diagram (as reference) for a portion of the Mg_2SiO_4-SiO_2 system from Bowen and Andersen (1914), Greig (1927), and Smith (1974). Abbreviations: Fo, forsterite; Pr, protoenstatite; En, orthoenstatite; Cr, cristobalite; Trid, tridymite; Qz, β-quartz; L, liquid.

It has been demonstrated that nucleation temperatures are confined to a specific range of undercoolings, a feature very much apparent by means of Fig. 17. If then the nucleation temperatures and the corresponding furnace temperatures are plotted, as in Fig. 18, it becomes evident that the spherules nucleating at the lowest temperatures are still tens of degrees above their ambient temperatures. This suggests that kinetics surrounding the nucleation of a crystalline phase from the metastable melt places definite limits on the temperature and undercoolings at which nucleation can occur. This means the initial conditions for crystal growth are also limited to a specific set of constraints established by nucleation kinetics for the experimental conditions provided.

Under the present experimental conditions the range of nucleation temperatures might very well be defined by the limits suggested in Fig. 18. It is of interest that this field seems to narrow and shift to higher temperatures and, also, lower undercoolings as a more forsterite-rich composition is approached. This is in agreement with experimental investigations performed on San Carlos peridot (no quantitative data available) demonstrating that a melt of olivine composition can be undercooled but to a relatively smaller degree for high cooling rates.

Nucleation Parameters

Bigg (1953) from an empirical approach and Price and Gornick (1967) from classical nucleation theory, have investigated parameters

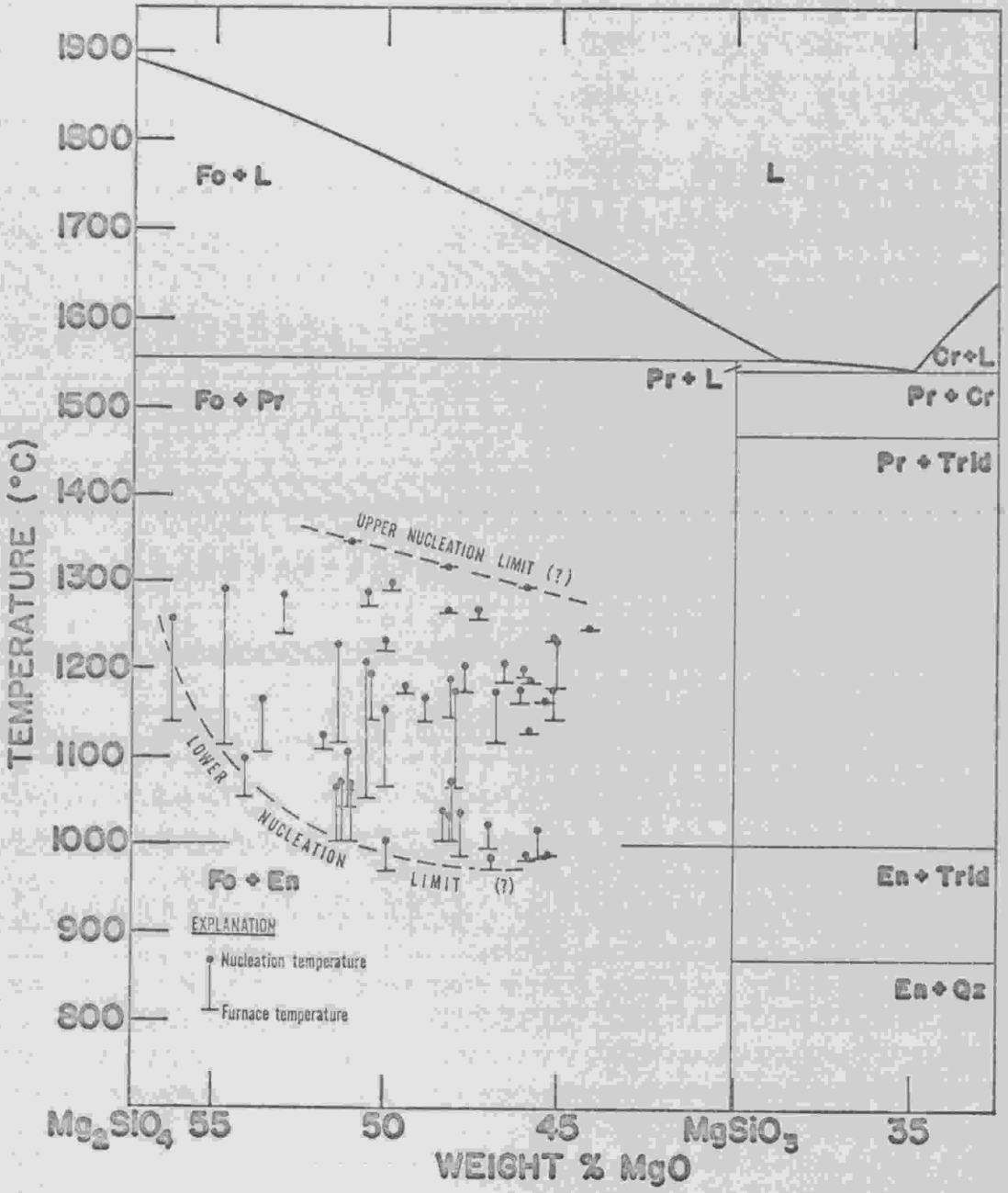

Fig. 18. Apparent temperature-composition limits for the nucleation of forsterite from undercooled magnesium silicate melts of this experimental investigation. Equilibrium phase diagram for a portion of the Mg_2SiO_4-SiO_2 system shown for reference. Abbreviations explained previously in Fig. 17.

surrounding nucleation of a crystalline phase from undercooled liquid droplets. Both of these investigators dealt exclusively with homogeneous nucleation and constant cooling rate processes. From their investigations it was shown that the maximum undercooling was dependent on the volume, composition, and the cooling rate of a droplet. Given a specific droplet volume and subjecting it to a constant cooling rate process provided a realm of temperatures in which nucleation would most probably occur. Such a probability curve is shown in Fig. 19 for a one millimeter diameter droplet of water cooling at 0.5°C/min. A droplet of water under these conditions would most likely nucleate ice in the temperature range from -19 to -27°C. The mean temperature of this interval (located at a probability of 0.5), for a specific cooling rate, was found to increase linearly with the logarithm of the diameter of the droplet. That is, larger droplets nucleated at higher temperatures (smaller undercoolings). Furthermore, for a specific droplet diameter, deeper undercooling could be achieved with higher cooling rates.

The breadth of the temperature interval in which nucleation occurs (Fig. 19) and its position with respect to the equilibrium liquidus under the present experimental conditions cannot be compared directly to the work of Bigg (1953) or Price and Gornick (1967) for the following reasons: First, the experiment includes a variety of droplet volumes. No attempt was made to experiment on a number of spherules of equal volume (or droplet diameter); secondly, it

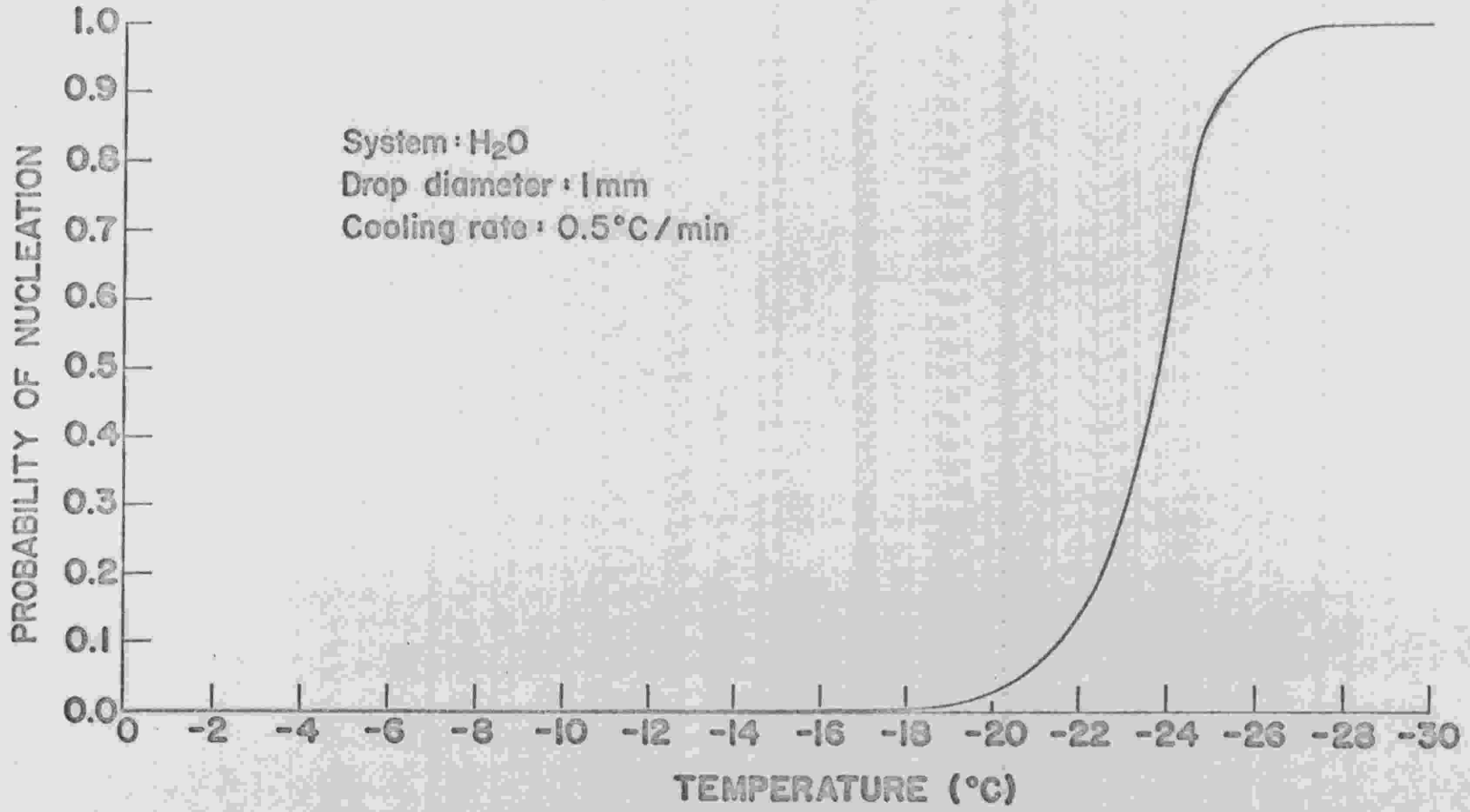

Fig. 19. The probability of nucleating ice from a 1 mm diameter droplet of water cooling at a rate of 0.5°C/min (after Bigg, 1953).

cannot be established whether nucleation was homogeneous or heterogeneous; thirdly, the cooling rates through which these spherules where subjected, must be considered.

The cooling rates that the magnesium silicate spherules encountered under the present experimental conditions can be obtained from their cooling curves (derived by Equation 9) as the $\lim_{\Delta\tau \to o} \frac{\Delta T}{\Delta \tau}$. Fig. 20 demonstrates the change in cooling rate of a 1 and 2 mm diameter droplet with respect to time as they cool from an initial temperature of 1800°C at laser turnoff to ambient temperatures of 950 to 1350°C. It is quite evident that immediately after laser turnoff the cooling rate is rather substantial and at least for the first second changes at a drastic rate. As might be expected, the cooling rates are not identical for different sized spherules under the same experimental conditions nor are they identical for the same sized spherule under different conditions. With the added complexities in these experiments by the variety of initial and ambient temperatures, it can be safely assumed that no two spherules of this experiment have encountered identical cooling histories. The fact that the cooling rates are not constant and that they are not similar between various spherules are probably the two decisive reasons why this experimental data cannot be compared directly to nucleation theory for molten droplets in the metastable state.

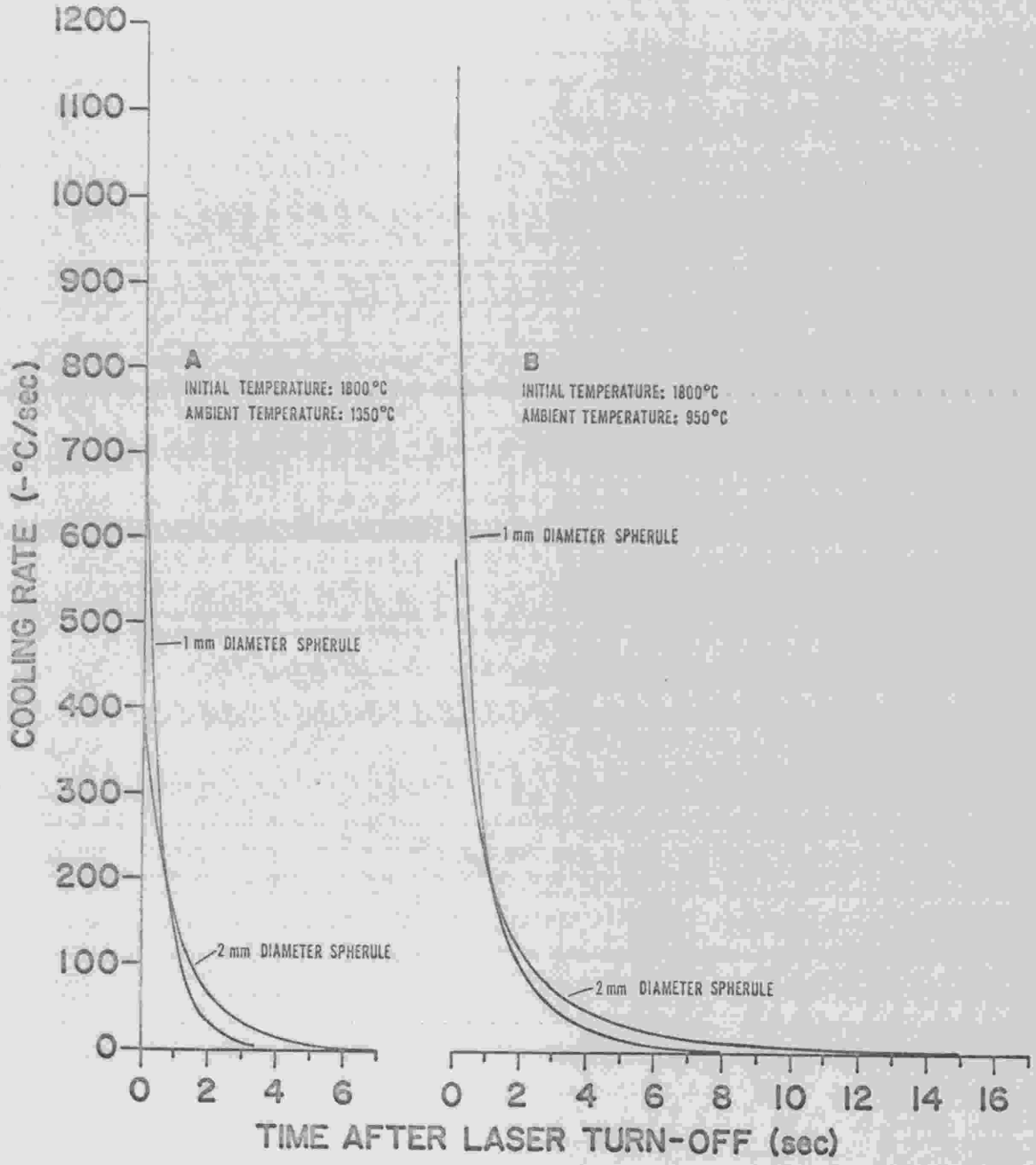

Fig. 20. The change in cooling rate with respect to time for 1 and 2 mm diameter magnesium silicate spherules with an initial temperature of 1800°C and an ambient temperature of either 1350°C (20a) or 950°C (20b).

Despite the fact that this experimental approach does not compare to that used to derive the nucleation theory, several general trends probably can be extended to the nucleation temperatures shown in Fig. 18. First, nucleation is most likely to occur within a range of temperatures corresponding to the physicochemical factors surrounding the event. Secondly, the breadth of this interval and its position with respect to the equilibrium liquidus should be expected to change with composition, droplet diameter, and cooling rates. This offeres an extremely wide range of initial conditions for the nucleation of a crystalline phase and for subsequent crystal growth. It also reveals the complexity in establishing the actual conditions surrounding chondrule formation considering the circumstances conceived by the numerous processes proposed to describe their origin. Thirdly, to further complicate the situation, an undercooled droplet could nucleate at any undercooling. The breadth of the nucleation temperature range is only that interval where nucleation is most likely to occur. The chances of nucleation outside this range is statistically small but not impossible.

It is believed that the limits sketched in Fig. 18, therefore, represent a composite of a multitude of limits established by the wide variety of conditions produced by these experiments.

Recalescence

The recalescence is brought about by the release of the heat of fusion as forsterite, the only phase nucleated in these experiments,

crystallizes from the undercooled melt. The affects most readily detected at this point are the increase in luminosity, in both the visible and infrared range and the increase in the temperature of the spherule. The recalescence, as demonstrated by Fig. 14, is marked by a sharp upward spike in the luminosity-time trace.

This event is important in the analysis of the experiment because most of the features observed in the quenched spherule result directly from the recalescence or through some subsequent thermal process acting on these primary features. Therefore, an understanding of the processes involved during this event can lead to the deciphering of those conditions present during the formation of chondrules.

A rigorous analysis of the recalescence process can be described as follows. As has been previously stated, the degree of undercooling achieved by the initial cooling process establishes the initial growth rate of forsterite at the time of nucleation. Through the crystallization of forsterite, the heat of fusion is released, thereby increasing the temperature of the spherule and consequently changing the degree of undercooling of the melt and the growth rate of the forsterite.

The rate at which the heat of fusion is released is dependent on the growth rate of the forsterite. The duration of time for which the energy will be released during the process becomes not only a function of the growth rate of the forsterite, but also a function of the volume of the melt that will be converted to the crystalline state during the course of the event.

The temperature of the spherule, as the event progresses, is dependent on the rate at which the heat of fusion is released, the average specific heat of the spherule, and the rate at which heat is being radiated at the surface. As a result, the maximum temperatures achieved during recalescence and the length of time required to reach that temperature become difficult to estimate.

Information collected on the recalescence event consists merely of visual time estimations. This information is given in Table 1. If the luminosity-time trace shown in Fig. 14 is representative of the thermal history of these spherules, despite the fact that the initial temperature, volume, and composition of the spherule it represents is unknown, the recalescence might be expected to last on the order of 65 msec. When the time estimates show in Table 1 are compared against the interval demonstrated by Fig. 14, it would appear that some basic assumption is very wrong. First, it has been demonstrated by means of Fig. 14 that this corresponding time interval represents a period too brief for a visual estimation. The shortest recalescence recorded in Table 1 is one-half second (500 msec.). Are the estimated intervals real? Secondly, for those spherules nucleating at a relatively low temperature, where the growth rate should also be relatively slow, an obvious luminosity peak might be hard to distinguish visually. Consequently, there should be some question as to the applicability of this data to subsequent analysis. Since no

attempt was made to measure the temperature of the spherules as a function of time during this event, other means must be attempted to help explain some of the observed features within the spherules.

Affect of the Recalescence Event on Crystal Morphology and Size

As heat is released by the growth of forsterite, the corresponding increase in temperature could expectedly bring about a change in crystal morphology and size. The sensitivity of these features with undercooling might then be demonstrated by superimposing them upon the nucleation temperatures as a function of composition. One should be aware, however, that the nucleation temperature represents only the initial temperature in this termal event.

Crystal Morphology. In Fig. 21 the observed crystal morphologies have been plotted on the estimated nucleation temperature of each of the spherules. A general systematic change in crystal morphology with the degree of undercooling for a given bulk composition is apparent from this diagram. With an increase in the degree of undercooling, for a given spherule bulk composition, the morphologies change from a bar-dendrite association, to dendrite-fiber, and fiber-submicroscopic associations, in that order. The devitrified spherules, with their submicroscopic crystals follow perfectly in this scheme. If then with increasing magnitude of undercooling the trend bars-dendrites-fibers-submicroscopic crystals were followed, the observed associations shown in Fig. 21 could be derived by

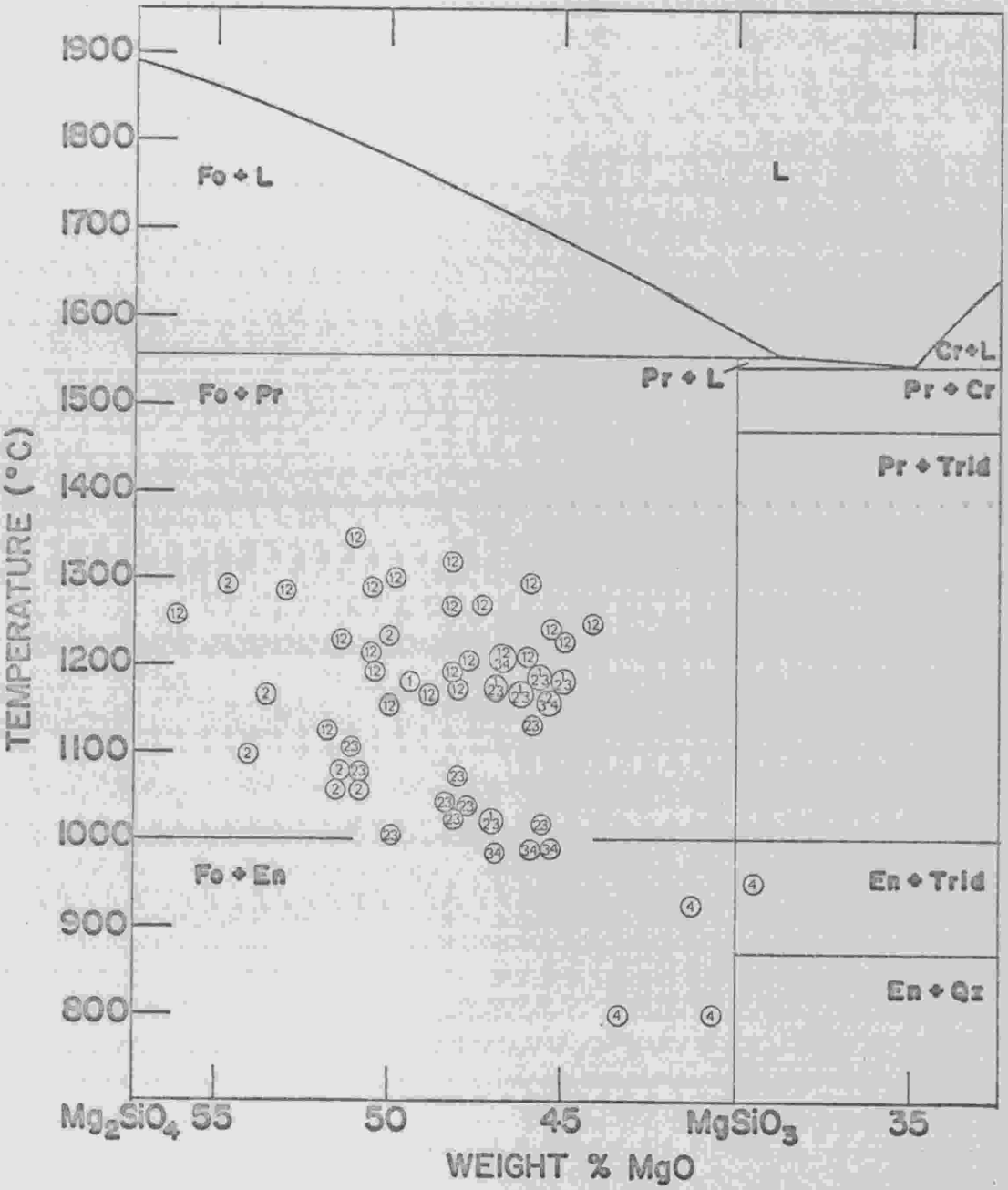

Fig. 21. Observed crystal morphologies superimposed on the nucleation temperature of the corresponding magnesium silicate spherules. Crystal morphologies: 1, bars; 2, dendrites; 3, fibers; and 4, submicroscopic crystals. Equilibrium phase diagram for a portion of the Mg_2SiO_4-SiO_2 system shown for reference. Abbreviations explained previously in Fig. 17.

accounting for the increase in temperature of the spherule during recalescence. This deduction correlates perfectly with those excentroradial spherules displaying the nucleation center, such as spherule 24E14 shown in Fig. 11. In spherule 24E14 the nucleation center is characterized by crystal fibers, corresponding to the crystallization of forsterite from the highly undercooled melt immediately after nucleation. As crystal growth continued and the temperature of the spherule had risen, the crystal morphology graded into crystal dendrites.

When the crystal morphologies, corresponding to the greatest undercooling of each of the spherules are plotted on their nucleation temperatures, composition-temperature limits can be established for the various morphologies. The crystal morphology fields as defined by this approach are presented in Fig. 22. It should be noted that only four of the spherules do not fit well to the morphology limits established in this figure. Three of these four spherules also do not fit according to crystal width classifications that will be discussed shortly. This suggests that some observation with respect to their nucleation temperature is probably incorrect.

From Fig. 22 it is apparent that the upper limit to the formation of submicroscopic crystals in the region of 45-47 wt. % MgO is approximately 1000°C, representing an undercooling on the order of 700°C. This boundary cannot be extended to a broader compositional

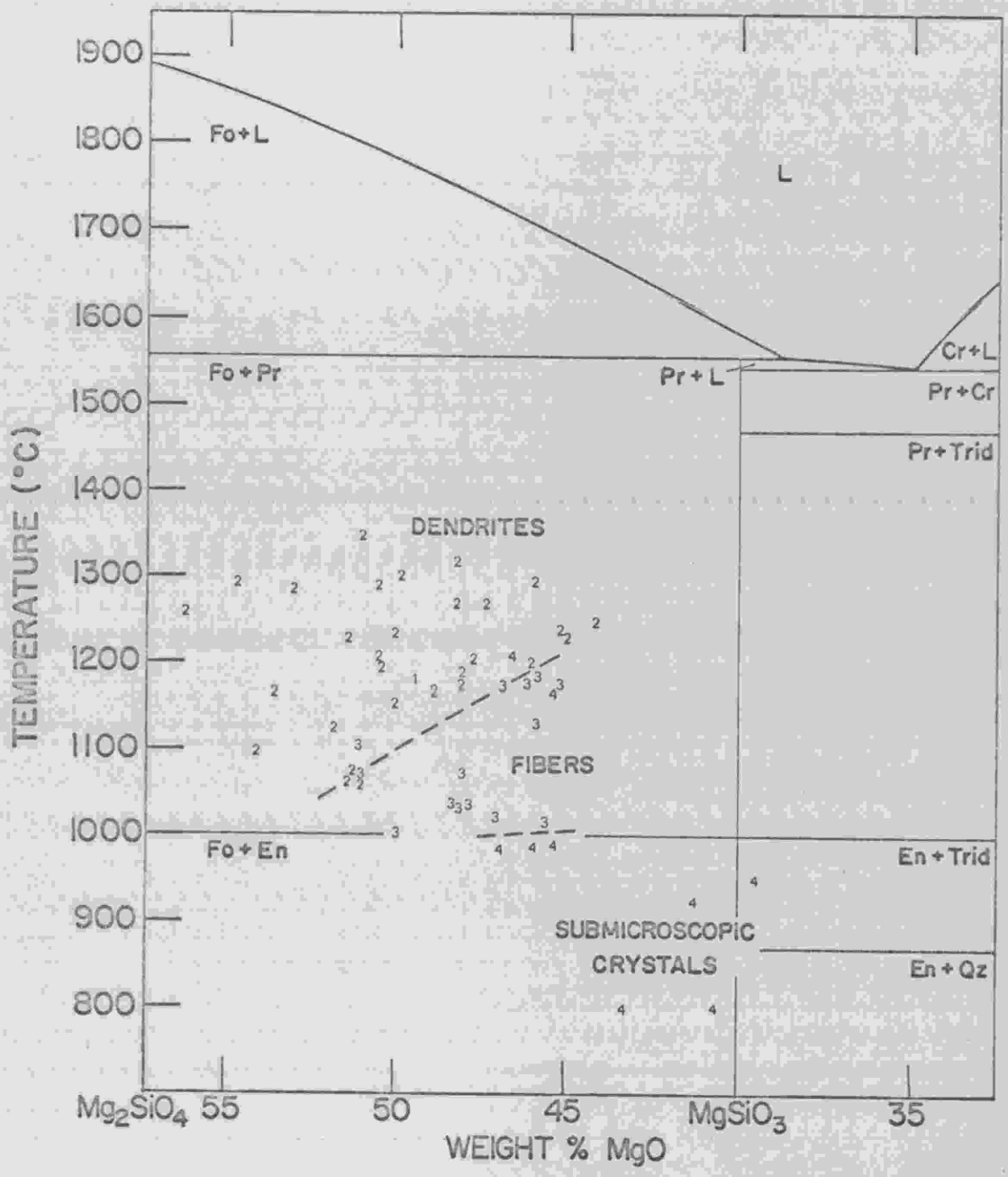

Fig. 22. The crystal morphologies that correspond to the nucleation temperatures of the magnesium silicate spherules. Crystal morphologies: 1, bars; 2, dendrites; 3, fibers; and 4, submicroscopic crystals. Dashed lines mark approximate limits to each morphology. Equilibrium phase diagram for a portion of the Mg_2SiO_4-SiO_2 system shown for reference. Abbreviations explained previously in Fig. 17.

range at this time. Its slope with respect to temperature and composition has not been established, however, it would appear that it is significantly smaller than that separating the dendrite and fiber morphology fields. The boundary separating the dendrite and fiber morphology fields extends from approximately 1200°C at 45 wt. % MgO to 1050°C at 52 wt. % MgO, cutting sharply across "iso"-undercooling curves (cf. Fig. 17).

Crystal size. To test the sensitivity of crystal width to undercooling, the crystal width classifications of each of the spherules have been plotted on their nucleation temperatures in Fig. 23. From this diagram there appears to be a decline in crystal width with greater undercooling only at lower nucleation temperatures.

Based on Fig. 12, which correlates crystal morphology with crystal width, and from the fact that crystal morphology goes from a bar shape to submicroscopic crystals with greater undercooling, there should be a general decline in crystal width with greater undercooling. This would suggest that the smallest crystal width present in any one spherule should conform to the undercooling at the time of nucleation. If then the crystal width classifications corresponding to the smallest crystal size for each spherule were plotted on their nucleation temperatures as a function of composition, limits on the extent of these classifications with respect to temperature and composition can be established. This information is presented by means of Fig. 24. It should be immediately evident

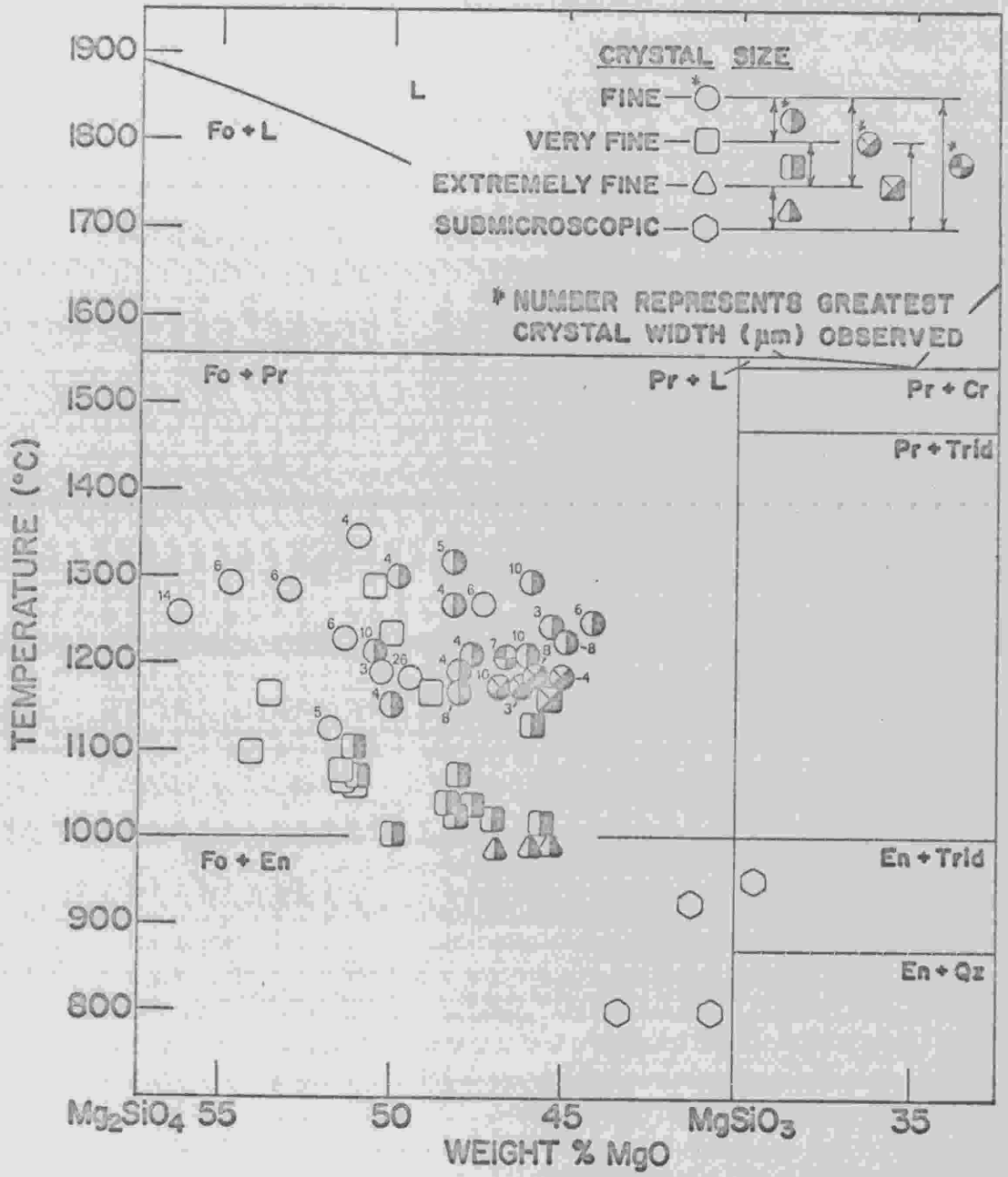

Fig. 23. Crystal width classifications superimposed on the nucleation temperatures of the corresponding magnesium silicate spherules. Range in crystal size given by appropriate symbol. Equilibrium phase diagram for a portion of the Mg_2SiO_4-SiO_2 system shown for reference. Abbreviations explained previously in Fig. 17.

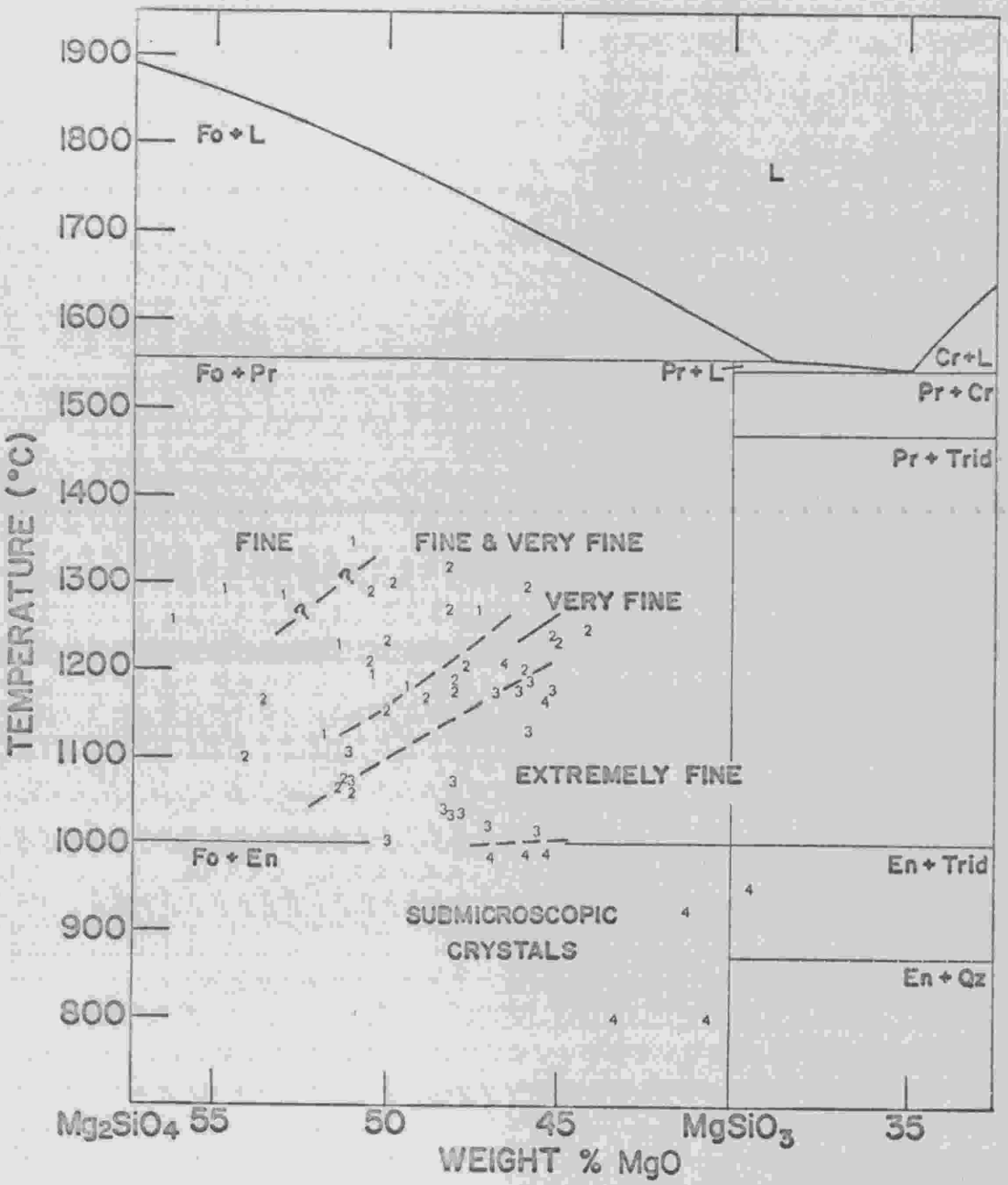

Fig. 24. Crystal width classes that correspond to nucleation temperatures of the magnesium silicate spherules. Crystal width classes: 1, fine; 2, very fine; 3, extremely fine; and 4, submicroscopic crystals. Dashed lines mark approximate limits to each class. Equilibrium phase diagram for a portion of the Mg_2SiO_4-SiO_2 system shown for reference. Abbreviations explained previously in Fig. 17.

that the boundaries between submicroscopic and extremely fine, as well as between extremely fine and very fine crystal classes are identical to those separating submicroscopic and fibers, and fibers from dendrites morphologies shown in Fig. 22 because of the way the crystal size classification has been established. Fig. 24 does demonstrate an additional boundary, one that separates very fine from a mixture of very fine and fine crystal width classes. At temperatures above this boundary there appears to be a relative insensitivity to which size class, fine or very fine, will first appear. There is a possibility, however, that an upper limit on this field does exist and crystal width may once again be directly correlateable to undercooling. This boundary cannot be established from the current data.

Comparison with Growth Rate Curve. The growth rate of forsterite is controlled by the degree of undercooling in a fashion shown by Fig. 25. As can be seen from this diagram, the growth rate increases sharply to a maximum as undercooling increases, just below the equilibrium liquidus temperature and then decreases rapidly and tapers off as the undercooling becomes even greater. It is believed that at nucleation the growth rate inherited by the forsterite, for all of the magensium silicate spherules studied, falls far to the right of the maximum shown by Fig. 25. This assumption can be supported if the corresponding states relationship for crystal growth rates, as outlined by Magill et al. (1973), can be used as a first approximation in this magnesium silicate system.

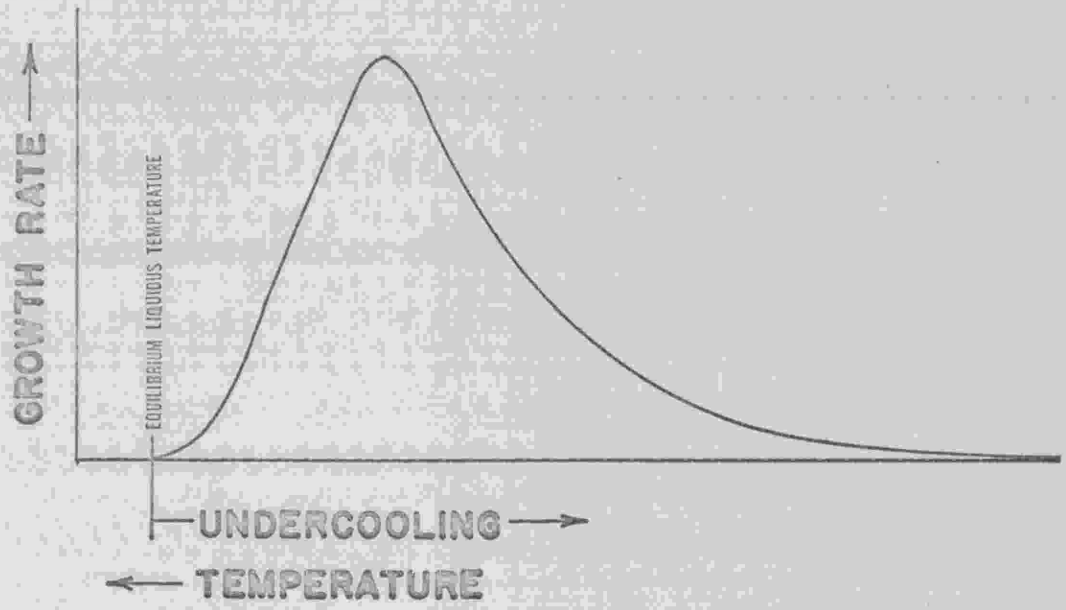

Fig. 25. A generalized growth rate curve.

The crystal morphology and size cannot be correlated directly to the growth rate curve since their trends have not been established for that region between the equilibrium liquidus and these nucleation temperatures, a region where the crystal growth rate makes a abrupt change with respect to undercooling. However, an interesting feature is generated if one would allow crystal morphology to be directly related to the growth rate curve while crystal size continued to increase with lesser undercooling. If the growth rate curve were followed, under these circumstances, from deep undercooling up toward the equilibrium liquidus the morphology trend might be submicroscopic fibers-fibers-dendrites-skeletal bars, and then possible bars with few skeletal features at the maximum growth rate for a given bulk composition. By letting the crystal size to increase further while allowing crystal morphology to follow the growth rate trend, a degeneration in morphology would be expected. That is, undercoolings less than that corresponding to the maximum growth rate would be expected to form large crystal dendrites. If nucleation continued to occur at the surface, as seems to be apparent for many of the magnesium silicate spherules studied, then the rim of the chondrule might represent the base of the crystal (the crystal body) from which large dendrites would extend into or through the central portion of the spherule. These crystal dendrites would be at approximately right angles to some specific crystallographic axis established in the rim. A barred chrondrule (or lamellar olivine

chondrule; Tschermak, 1885), where the olivine consists of a single, optically congruent crystal (or several crystals if more than one nucleation center were involved), might then represent nucleation at a very shallow undercooling. This suggestion, however, remains to be tested experimentally.

Range in Crystal Morphology and Size. In addition to the trends previously observed in Figs. 21 and 23, there is another feature apparent in both of these figures. The range in crystal morphology and size that can exist in any given spherule tends to increase with a more silica rich bulk composition. The nature of this phenomena is not obvious, but may reflect a change in the growth rate curve of forsterite with respect to bulk composition. This would, undoubtedly, be expected considering the diffusion of material to and from the growing crystal faces of forsterite within spherules of initially high silica content.

Forsterite-Melt Relationship

Since forsterite is the only phase nucleated from the melt, its crystallization forces the melt to become more silica-rich thereby maintaining a mass balance between forsterite, melt, and the bulk composition. Electron microprobe point beam analysis on the glass phase (interpreted as being quenched residual melt) for the seven spherules listed in Table 3 shows that, at least for these seven

spherules, forsterite will continue to crystallize until the melt composition coincides with that of the eutectic in the forsterite-silica system.

The amount of each phase present in the seven spherules for which the glass composition is known, can be determined from a mass balance between forsterite, glass, and bulk composition. The percentage of each phase present is listed in Table 5. It is apparent that large quantities (34 to 54 wt. %) of each of these spherules remains as glass.

If it were assumed that the final glass composition in all of the magnesium silicate spherules formed in this experiment correspond to that of the eutectic, a statement that cannot be proven from available data, then a spherule with a forsterite bulk composition would be expected to crystallize to pure forsterite without any glass, that is, the spherule would truely be monomineralic. However, a spherule of enstatite composition, nucleating only forsterite, would contain 77 wt. % glass. If extended to the other extreme, a spherule of eutectic composition would not be expected to nucleate even forsterite and would consist entirely of glass.

Maximum Temperature Increase

The maximum increase in the temperature of the spherule can be estimated for the seven spherules listed in Table 3 based on thermodynamic data provided by Barin and Knacke (1973) and assuming the recalescence to be an adiabatic process. This increase in

Table 5. The amount of forsterite and glass present in the seven spherules for which the residual melt composition is known.

SPHERULE	BULK COMPOSITION (wt %)			PHASE ASSEMBLAGE (wt %)	
	SiO_2	MgO	Total	Fo	Gl
E5	55.8	45.1	100.9	46.5	53.5
24E11	53.9	45.6	99.5	48.7	51.3
EM	54.2	45.9	100.1	50.0	50.0
ET	53.4	46.0	99.4	50.4	49.6
23E2	52.6	46.8	99.4	53.9	46.1
23E7	51.5	48.0	99.5	59.2	40.8
EG	50.4	49.4	99.8	65.4	34.6

Fo = forsterite; Gl = glass interpreted to be quenched residual melt.

temperature is estimated to be on the order of 180 to 255°C above their nucleation temperatures depending upon the spherule. The temperature difference between nucleation and peak recalescence is shown diagramatically in Fig. 26 by means of tie-lines between initial melt composition (at nucleation) and the eutectoid glass. It is evident from this figure that these spherules never reach any portion of the equilibrium liquidus during the recalescence. The fact that the residual glass has a composition corresponding to that of the eutectic cannot be explained at this time.

Curved Crystal Dendrites

There are additional observations which are directly linked to the thermal history of the spherules but do not directly evolve from previous considerations.

The first such observation deals with curved crystal dendrite growth displayed in spherules that have nucleated at relatively low temperatures. This phenomenon has recently been studied by Knight (1971) for a variety of materials and his observations appear pertinent to the magnesium silicate spherules of the present study.

According to Knight (1971) the general trend of crystallization behavior can be demonstrated by Fig. 27. At relatively low undercoolings the crystal form is needle-like, a form controlled by the relatively

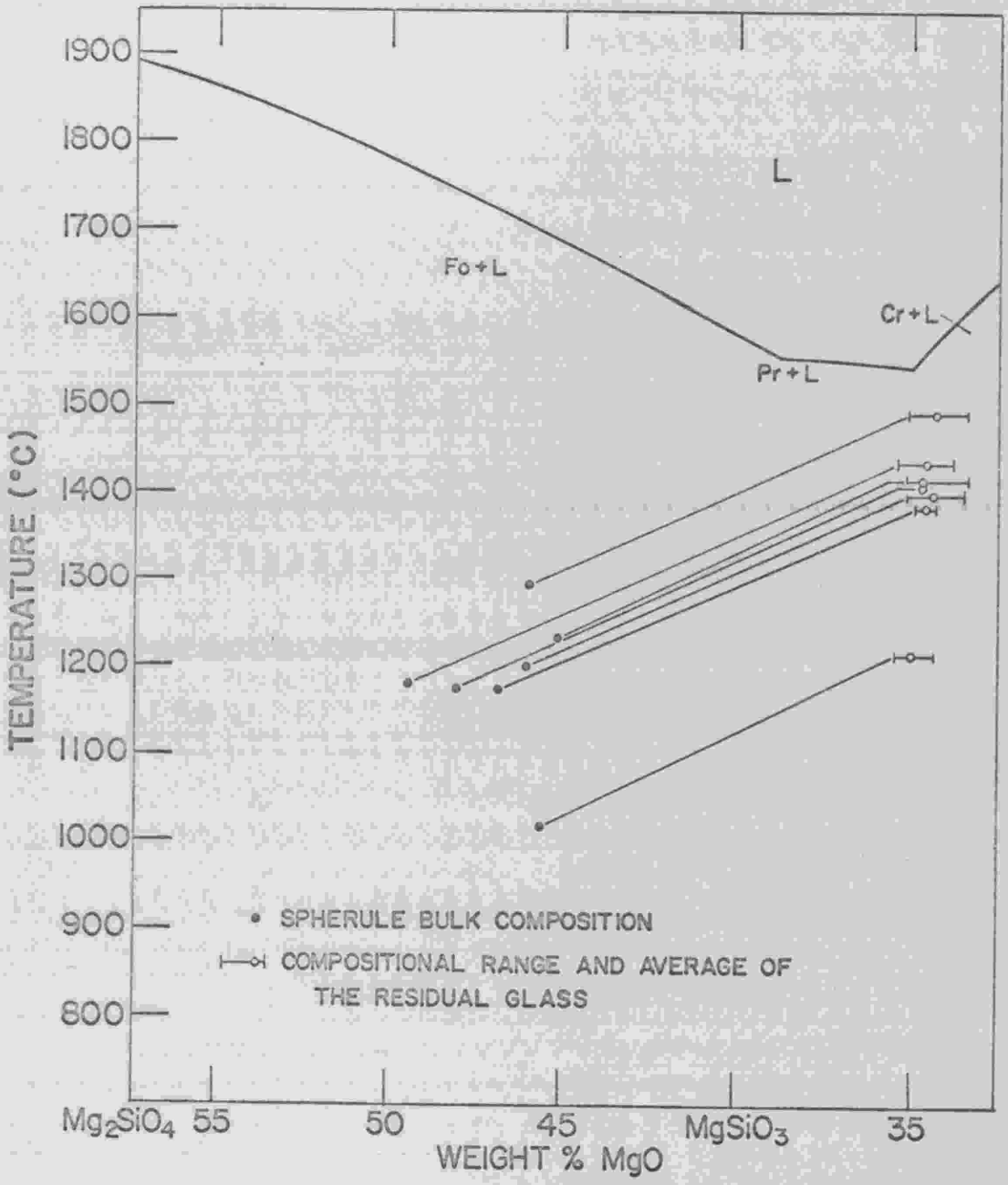

Fig. 26. Nucleation temperatures, estimated maximum peak recalescence temperatures, and their corresponding melt compositions marking the initiation and termination of the recalescence event for the seven spherules listed in Table 3. Equilibrium liquidus for a portion of the Mg_2SiO_4-SiO_2 system from Bowen and Andersen (1914) and Greig (1927). Abbreviations explained previously in Fig. 17.

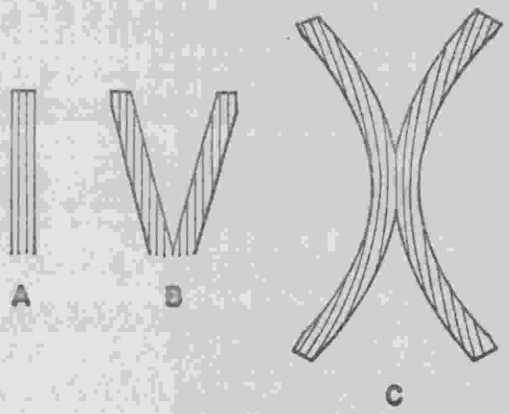

Fig. 27. Illustration of needle and dendrite growth with decreasing temperature (increasing undercooling) of the crystallization of materials that form curved dendrites. At low undercooling the growth is by needles (27a). With increasing undercooling the dendrite axis orientation changes continuously (27b) and curvature starts in the sense given in 27c (after Knight, 1971).

slow growth of the crystal sides. With increasing initial undercooling the fast growth direction, i.e. the tips of the needle, forms a succession of completely coherent but elastically strained nuclei. That is, the onset of curved dendrite growth coincides with the dendrite orientations becoming non-rational crystallographic directions. The observed effect is that the fast growth direction begins to rotate away from the initial orientation, parallel to the slowest-growing faces, allowing the dendrites to grow more rapidly then they would if they continued the self epitaxial relation provided by the formation of a straight dendrite. The overall result is a curved crystal which is curved in shape and consists of a curved crystal lattice. The elastic strain can often be relaxed just about as fast as it can form. In those cases where it does not relax, Knight (1971) suggests that the viscosity of the residual fluid (or melt) could keep the crystals from straightening out.

Textures

The second observation that does not directly evolve from previous considerations of the thermal history of the spherules is the overall texture in a spherule resulting from the present experimental conditions.

The Excentroradial Texture

Textures, as observed directly from thin section view, have been classed previously in Table 1. Examination of those spherules

displaying excentroradial textures reveals that there is a definite restriction placed on their grain morphology. These grains are wedge-shaped with their two diverging sides radiating from the nucleation center. In three dimensional perspective, a single grain within a spherule would appear similar to that pictured in Fig. 28a, where, in this case, the nucleation center lies at the back of the spherule at the intersection of planes 1 and 2. Planes passing through such a spherule at right angle orientations shown in the diagram, as to represent thin section views, produce two varieties of the excentroradial texture (Figs. 28b and c) which have not been differentiated in Table 1, and a third texture that is not excentroradial, here displayed as Fig. 28d.

When considering more than one grain in these spherules, it is commonly found that the grain boundaries diverging from the nucleation center are often the common boundary of two similarly oriented grains. That is, the grains are often stacked next to each other. However, it is not uncommon to find grains, each radiating from the same nucleation center, that are oriented in such a manner that the grains intersect each other at some angle. Such can be represented by Fig. 29a. In this case, a plane passed through the spherule as shown in this diagram would result in a texture demonstrated by Fig. 29b, which is also not an excentroradial texture.

If then Figs. 28 and 29 were compared to those spherules displaying a parallel grain texture (Fig. 5) a marked similarity is

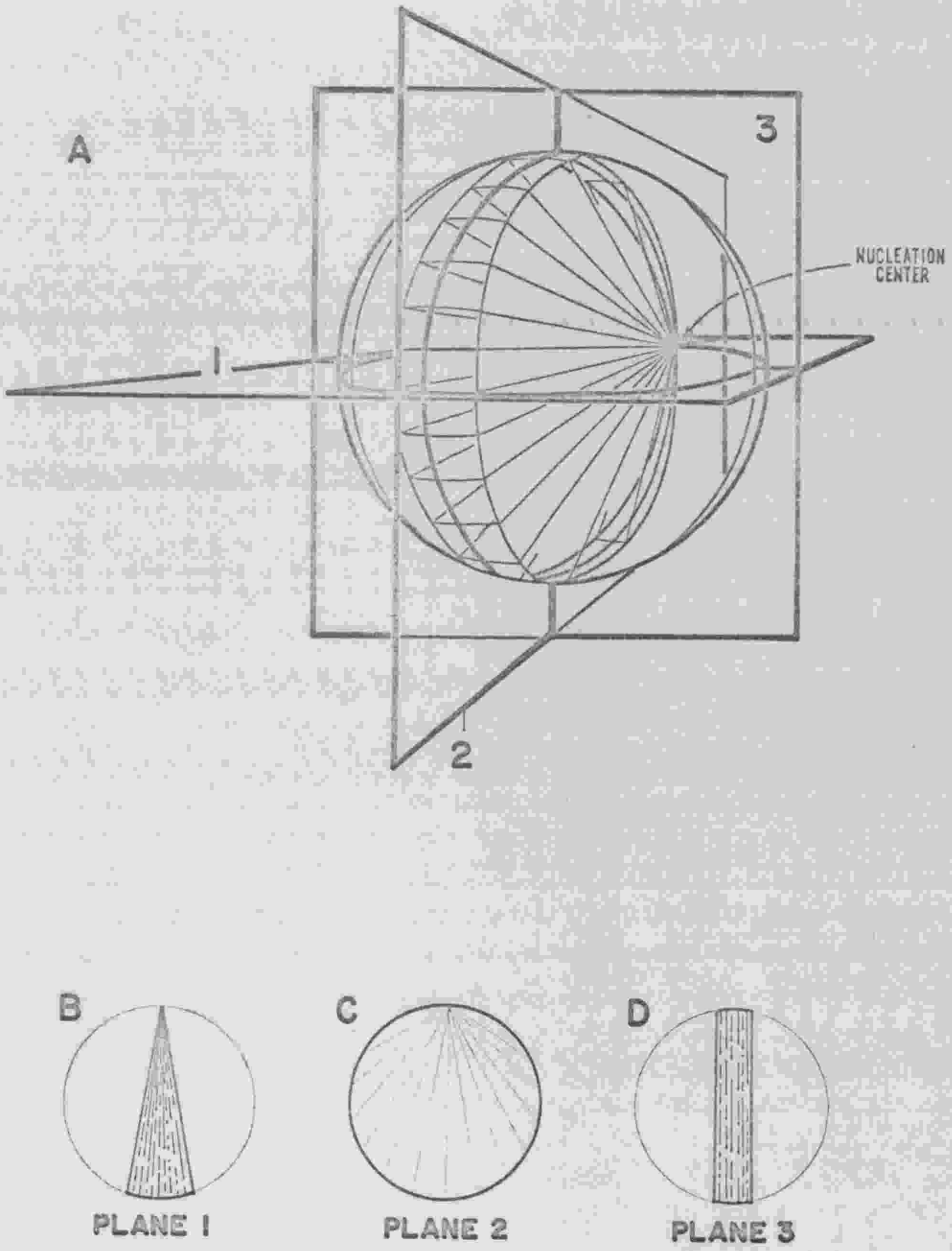

Fig. 28. Diagram illustrating the derivation of two types of excentroradial texture and a third texture that is not excentroradial from a spherule containing a single wedge-shaped grain. Grain boundaries shown in 28b-d represent thin section views along planes 1-3, respectively.

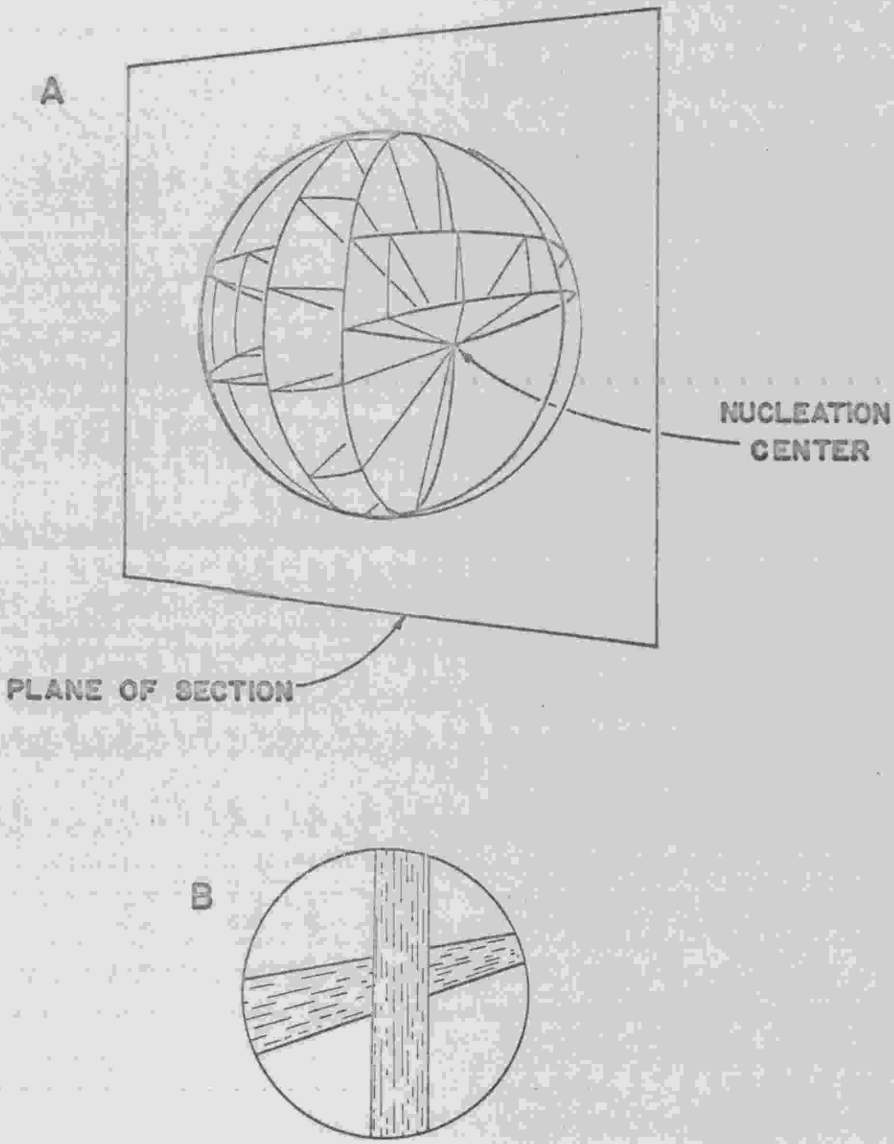

Fig. 29. Diagram of a spherule containing two wedge-shaped grains (29a), each radiating from the same nucleation center but oriented at some angle to each other, and the texture (29b) resulting from a plane passed through the spherule as shown.

apparent. Most of those spherules classed as parallel grain textures are found to be a derivative of excentroradially-arranged, wedge-shaped grains. These textures could become quite complex if numerous nucleation centers would happen to form at approximately the same time near the surface of the spherule. Those spherules displaying a random grain or radial texture, however, appear to have little genetic relation to those grouped as excentroradial derivatives.

Textures as a Function of Nucleation Temperatures

A reclassification of textures based on the above concept is given in Table 6. This revised classification has also been superimposed on the nucleation temperatures in Fig. 30.

It can be seen from Fig. 30 that the spherulitic texture can generally be separated from all other textures, occupying the greatest undercoolings for any given bulk composition. The upper limit of this texture is observed to shift to higher nucleation temperatures with increasing silica bulk content of the spherule.

Of the remaining textures, the majority are excentroradial derivatives followed by radial and random grain textures, in that order. Those textures defined as excentroradial derivatives are common at any nucleation temperature created by these experiments except at temperatures below the upper limit established by the spherulitic texture. The radial texture is generally found at nucleation temperatures adjacent to the spherulitic region and

Table 6. Revised textural classification of the magnesium silicate spherules. Revision based on the concept of excentroradially-arranged, wedge-shaped grains observed in spherules displaying an excentroradial texture.

SPHERULE	TEXTURE	SPHERULE	TEXTURE
EB	E	23E2	E
EC	E	23E3	E
ED	R	23E4	E
EE	E	23E5	E
EG	E	23E6	E
EH	E	23E7	E
EI	E	23E8	R(?)
EK	RG	23E9	E
EL	E	23E12	R
EM	E	24E1	E
EN	RG	24E2	R
EP	R	24E3	E
EQ	RG	24E4	E
ER	E	24E5	E
ET	E	24E6	R
E1	E	24E7	R
E2	E	24E8	S
E3	RG	24E9	S
E4	RG	24E10	E
E5	E	24E11	R
E7	E	24E12	S
E13	E	24E13	S
E18	E	24E14	E
E20	E	MB1	S
E21	S	MB2	S
E26	S	MB5	S
23E1	E(?)	MB6	S

EXPLANATION

E Derivative of the excentroradial texture

R Radial texture

RG Random grain texture

S Spherulitic texture

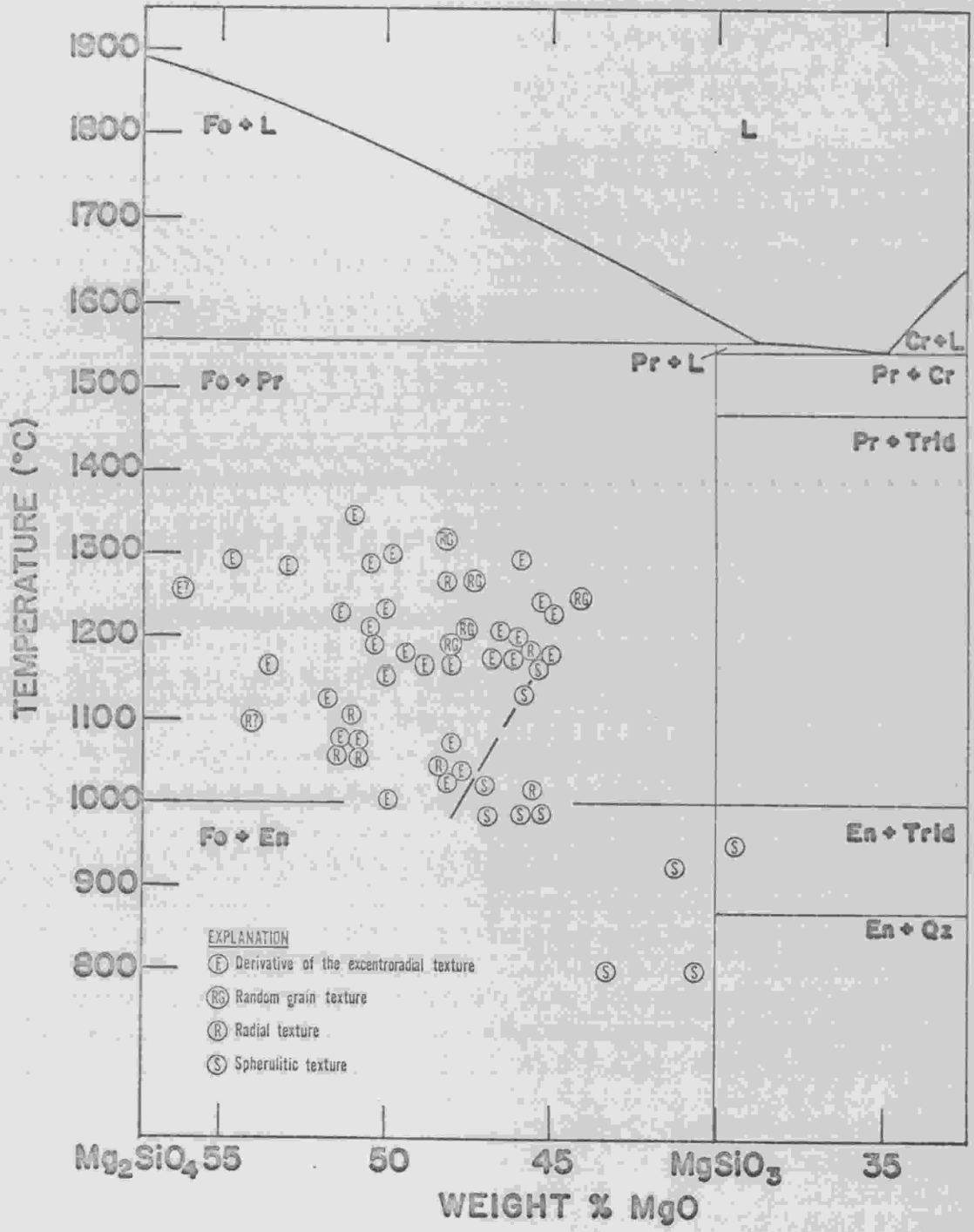

Fig. 30. The textures displayed in the magnesium silicate spherules superimposed on corresponding nucleation temperatures. Dashed line generally separates the spherulitic texture from all other textures shown. Equilibrium phase diagram for a portion of the Mg_2SiO_4-SiO_2 system shown for reference. Abbreviations explained previously in Fig. 17.

coexists with the excentroiadial derivatives. The random grain texture occupies high nucleation temperatures but does not form a distinctive pattern with respect to composition.

It should be noted that upper temperature limits have not been established for most of these textures. Therefore, a chondrule (with a composition close to the forsterite-silica join) displaying an excentroradial texture may not necessarily have nucleated at temperatures below 1300°C. In addition, since textures that are excentroradial derivatives occupy a wide range of nucleation temperatures, e.g. at least a 300°C interval at 50 wt. % MgO, texture alone is not a good indicator of the degree of undercooling achieved before nucleation.

Nucleation Near the Surface of the Spherule

Since the majority of the spherules that have been formed under these conditions produce a texture that is an excentroradial derivative, it is necessary to make a comment pertinent to the location of their nucleation center. Up to the present discussion temperature distribution within a spherule has been considered approximately uniform throughout. As long as the internal resistance to heat flow within the spherule is negligible, the above assumption is valid. If, however, the resistance to heat flow is small, but not negligible, as it could possibly be under present experimental conditions, the temperature distribution within the spherule would

not be uniform. That is, since heat flow would not be capable of responding to a high heat transfer across the boundary of the system, the surface should be the coolest portion of the spherule. This effect would be enhanced with still greater cooling rates, however, can also be dampened by convection of the melt within the spherule. Placing quantitative values on these effects is difficult at this time.

No matter whether nucleation of the spherule is homogeneous or heterogeneous, it has been demonstrated by means of Fig. 18 that nucleation is most likely to occur within a limited range of undercooling. If then the spherules surface is cooler than its interior, the surface should enter this nucleation region ahead of the rest of the spherule and have a leading chance to nucleate a crystalline phase.

For the case where nucleation occurs at the iridium wire-melt interface, heat conducted away from the spherule by conduction through the iridium wire support should also produce a similar effect as described above.

On Deciphering the Thermal History of Chondrules

Crystal morphology, crystal width, and texture provide definite trends with respect to nucleation temperature and bulk composition. Singularly or in combination with each other, these features can be compared against Figs. 22, 24 and/or 30 to establish specific limits

to the nucleation temperature of an undercooled droplet or of a chondrule. Alone, however, a feature such as the texture of a spherule or chondrule, may not be a good indicator of nucleation temperature because of the range in conditions under which it can be produced.

Once limits on the nucleation temperature of a chondrule have been established, specific physiocochemical parameters, such as cooling rate, can be sought that would restrain nucleation until such an undercooling has been reached. This provides a means to test various models that attempt to explain the formation of chondrules. It cannot be determined specifically how volume, composition, or rate of cooling would effect nucleation kinetics for these spherules based on present experimental techniques. The general trends that might be expected with a variation in any of these parameters has been based principally on the theory as derived by Bigg (1953) and Price and Gornick (1967).

Crystal morphology, crystal width and the melt composition have been shown to change during recalescence. General trends have been established for these features as a function of the temperature increase during this thermal event, however, specifically how they change with temperature and with the forsterite-melt relationship during crystallization and, also, exactly what properties control these features, thermodynamic or otherwise, has not been determined.

Of the features resulting directly from the recalescence, the mineralogy of a chondrule may become a very useful tool in establishing the nucleation parameters once crystallization processes in metastable melts is better understood.

There are chondrules or fragments thereof that, at least, superficially resemble the magnesium silicate spherules produced under the present experimental conditions, however, unless their bulk compositions lie near the forsterite-silica join, erroneous conclusions may result when comparing their features to those of this experiment. At least one additional oxide component of significant amount is present in nearly all chondrules. Such would change the equilibrium liquidus temperature and, consequently, the degree of undercooling characteristic of specific nucleation features (i.e. crystal morphology, etc.). Distinct crystal morphologies and/or crystal widths may also shift with respect to nucleation temperature in multicomponent-silicate systems. In addition, a spherule or chondrule that has nucleated another phase instead of or coincidental with forsterite could signify a totally different set of parameters governing the nucleation of that particular chondrule.

Since a single meteorite usually displays a wide variety of chondritic features, gross errors in the interpretation of the possible modes of chondrule formation and subsequent history can be avoided if the physiochemical conditions can be determined to explain

all features observed in chondrules of that meteorite. Such an analysis cannot be attempted based on available experimental data.

CONCLUSIONS

1) Magnesium silicate spherules resulting from these high cooling rate experiments, consist entirely of forsterite and a glass. Although nucleation occurs within the forsterite-protoenstatite field of the equilibrium phase diagram, nucleation of enstatite polymorphs is suppressed. The glass phase, for seven spherules in which it could be analyzed, is of eutectic composition for the forsterite-silica system.

2) For a given bulk composition, forsterite crystal morphology is a function of temperature and, consequently, the degree of undercooling. With greater degrees of undercooling the morphology follows the order: bars-dendrites-fibers-submicroscopic crystals. The range in crystal morphologies observed in any one spherule reflects the increase in temperature during recalescence.

3) Crystal size, based on a crystal width classification, generally decreases with larger degrees of undercooling for a given bulk composition. At the higher nucleation temperatures of this experiment there appears to be a relative insensitivity to which size class, fine or very fine, will first appear.

4) Spherules displaying an excentroradial texture consist of wedge-shaped grains that radiate from the nucleation center. These grains may be stacked next to each other or have some cross-cutting relationship with other grains. Planes passed through such spherules,

as to represent a thin section view, can generate textures which are not excentroradial.

5) Spherules displaying a spherulitic texture nucleated at temperatures lower than those spherules displaying any other texture, for a given bulk composition. Of the remaining textures, excentroradial derivatives are by far the most abundant, occuring at all nucleation temperatures resulting from this experiment, greater than those of the spherulitic texture.

6) Within specific temperature limits, diagrams in which crystal morphology, crystal width and texture have been correlated with nucleation temperature and bulk composition, are potential references for the determination of chondrule nucleation temperatures.

7) There is a temperature realm in which nucleation of a metastable melt, whether homogeneous or hetrogeneous, is most likely to occur. Once the limits on the nucleation temperature of a chondrule are known, specific physicochemical parameters (e.g. cooling rate) can be sought that would restrain nucleation until such undercoolings have been reached. This provides a means to test various models that attempt to explain chondrule formation.

8) Curved crystal dendrites, observed in many of the highly undercooled spherules, allows the forsterite to grow more rapidly than it would if it continued with a straight crystal dendrite form.

9) For those spherules displaying a texture which is derivative of excentroradially-arranged, wedge-shaped grains, the forsterite

appears to be nucleating from the coolest portion of the spherule, that is, the surface or iridium wire-melt interface.

10) Unless the bulk composition of a chondrule lies near the forsterite-silica join, erroneous conclusions may result when comparing its internal features to those of this experiment. The present experiment offers little insight into how the various features within magnesium silicate spherules might shift with respect to temperature and undercooling in a multicomponent silicate system.

REFERENCES

Albee, A. L., and L. Ray, 1970. Correction factors for electron probe microanalyses of silicates, oxides, carbonates, phosphates and sulfates. Anal. Chem., 42, 1408-1414.

Barin, I., and O. Knacke, 1973. Thermodynamic properties of inorganic substances. Springer-Verlag, New York, 921 p.

Bence, A. E., and A. L. Albee, 1968. Empirical correction factors for the electron microanalysis of silicates and oxides. J. Geol., 76, 382-403.

Bigg, E. K., 1953. The supercooling of water. Proc. Phys. Soc., B66, 688-694.

Blander, M., and M. Abdel-Gawad, 1969. The origin of meteorites and the constrained equilibrium theory. Geochim. Cosmochim. Acta, 33, 701-716.

Blander, M., and J. L. Katz, 1967. Condensation of primoidial dust. Geochim. Cosmochim. Acta, 31, 1025-1034.

Bowen, N. L., and O. Andersen, 1914. The binary system MgO-SiO_2. Amer. Jour. Sci., 37, 487-500.

Frederiksson, K., 1963. Chondrules and the meteoritic parent bodies. Trans. N. Y. Acad. Sci., 25, 765-769.

Frederiksson, K., 1969. The Sharps chondrite-new evidence on the origin of chondrules and chondrites. In: P. M. Millman, ed., Meteorite Research, p. 155-165. Reidel, Dordecht.

Fredriksson, K., and A. M. Reid, 1965. A chondrule in the Chainpur meteorite. Science, 149, 856-860.

Fredriksson, K., and A. E. Ringwood, 1963. Origin of meteoritic chondrules. Geochim. Cosmochim. Acta, 27, 639-641.

Fredriksson, K., J. Nelen, and W. G. Melson, 1970. Petrology and origin of lunar breccias and glasses. Proc. Apollo 11 Lunar Sci. Conf., Geochim. Cosmochim. Acta, Suppl. 1, 1, 419-432.

Greig, J. W., 1927. Immiscibility in silicate melts. Amer. Jour. Sci., 13, 1-44.

Keil, K., 1967. The electron microprobe x-ray analyzer and its application in mineralogy. Fortschr. Mineral., 44, 4-66.

Keil, K., G. Kurat, M. Prinz, and J. A. Green, 1972. Lithic fragments, glasses and chondrules from Luna 16 fines. Earth Planet. Sci. Lett., 13, 243-256.

King, E. A., M. F. Carman, and J. C. Butler, 1972. Chondrules in Apollo 14 samples: implications for the origin of chondritic meteorites. Science, 175, 59-60.

Knight, C. A., 1971. Breeding of crystal nuclei by classical nucleation: theory and some observations and experiments. Jour. Crystal Growth, 11, 201-217.

Kurat, G., K. Fredriksson, and J. Nelen, 1969. Der Meteorit von Siena. Geochim. Cosmochim. Acta, 33, 765-773.

Kurat, G., K. Keil, M. Prinz, and C. E. Nehru, 1971. Chondrules of lunar origin (abstract). Meteoritics, 6, 285.

Kurat, G., K. Keil, M. Prinz, and C. E. Nehru, 1972. Chondrules of lunar origin. Proc. Third Lunar Sci. Conf., Geochim. Cosmochim. Acta, Suppl. 3, 1, 707-721.

Magill, J. H., H. M. Li, and A. Gandica, 1973. A corresponding states equation for crystallization kinetics. Jour. Crystal Growth, 19, 361-364.

Merrill, G. P., 1920. On chondrules and chondritic structure in meteorites. Proc. Nat. Acad. Sci., 6, 449-472.

Nelson, L. S., M. Blander, S. R. Skaggs, and K. Keil, 1972. Use of a CO_2 laser to prepare chondrule-like spherules from supercooled molten oxide and silicate droplets. Earth Planet. Sci. Lett., 14, 338-344.

Price, F. P., and F. Gornick, 1967. Estimation of nucleation parameters from continuous cooling droplet experiments. Jour. Applied Phys., 38, 4182-4186.

Prinz, M., T. E. Bunch, and K. Keil, 1971. Composition and origin of lithic fragments and glasses in Apollo 11 samples. Contri. Mineral. Petrol., 32, 211-230.

Ringwood, A. E., 1961. Chemical and genetic relationships among meteorites. Geochim. Cosmochim. Acta, 24, 159-197.

Rinne, F., 1895. Ueber rhombishen Augite als Contactproduct, chondrenartige Bildungen aus künstlichen Schmelzen und über Concretionen in Basalten. Neues Jahrbuch der Mineralogie, Geol., und Paläont., 11, 229-246.

Rinne, F., 1897. Kugerlrunde Eiskrystalle und Chondren von Meteoriten. Neues Jahrbuch der Mineralogie, Geol., und Paläont., 11, 259-261.

Salisbury, W. W., and D. F. Fernald, 1970. Experimental chondrule formation (abstract). Meteoritics, 5, 220.

Sears, F. W., and M. W. Zemansky, 1967. University Physics. Addison-Wesley Pub. Co., Reading, 1028 p.

Smith, J. R., 1974. Experimental study on the polymorphism of enstatite. Amer. Mineral., 59, 345-352.

Sparrow, E. M., and R. D. Cess, 1970. Radiation heat transfer. Wadsworth Pub. Co., Inc., Belmont, 340 p.

Tomlinson, J. W., M. S. R. Heynes and J. O'M. Bockris, 1958. The structure of liquid silicates: part 2 - molar volumes and expansivities. Faraday Soc. Trans., 54, 1822-1833.

Tschermak, G., 1875. Die mikroskopische Beschaffenheit der Meteoriten. Trans. by J. A. Wood and E. M. Wood, 1964. Smithsonian Contributions to Astrophysics, 4, no. 6, 239 p.

Urey, H. C., 1967. Parent bodies of the meteorites. Icarus, 7, 350-359.

Wahl, W., 1952. The brecciated stony meteorites and meteorites containing foreign fragments. Geochim. Cosmochim. Acta, 2, 91-117.

Whipple, F. L., 1966. Chondrules: suggestions concerning the origin. Science, 153, 54-56.

Wood, J. A., 1963a. On the origin of chondrules and chondrites. Icarus, 2, 152-180.

Wood, J. A., 1963b. Chondrites and chondrules. Scientific American, 209, 65-82.